UNIVERSITY OF OKLAHOMA

GRADUATE COLLEGE

SELF-DIVERTING NANOPARTICLE BASED IN-SITU GELLED ACIDS FOR STIMULATION OF CARBONATE FORMATIONS

A DISSERTATION

SUBMITTED TO THE GRADUATE FACULTY

in partial fulfillment of the requirements for the

Degree of

DOCTOR OF PHILOSOPHY

By

SANGHO BANG
Norman, Oklahoma
2017

Downloaded from SHAREOK. Persistent Handle URL: https://hdl.handle.net/11244/54299

SELF-DIVERTING NANOPARTICLES-BASED IN-SITU GELLED ACIDS FOR STIMULATION OF CARBONATE FORMATIONS

A DISSERTATION APPROVED FOR THE
MEWBOURNE SCHOOL OF PETROLEUM & GEOLOGICAL ENGINEERING

BY

_____
Dr. Bor-Jier (Ben) Shiau, Chair

_____
Dr. Jeffrey H. Harwell

_____
Dr. Maysam Pournik

_____
Dr. Ahmad Jamili

_____
Dr. Ahmad Ramadan

© Copyright by SANGHO BANG 2017
All Rights Reserved.

DEDICATION

I dedicate my dissertation work to my family and many friends. A special feeling of gratitude is given to my loving parents, Junsu Bang and Youngsoon Kim who have unconditional love to their son and offered endless support for me throughout their life. I cannot thank them enough for all their deep devotion to my life journey. My brother Sangje Bang has never left me aside and is a very special gift from God.

I also dedicate this dissertation to my lifelong friends and my advisors who have supported me throughout the process. I will always appreciate all they have done, especially Dr. Shiau and Dr. Harwell for helping me to become a wiser man with love, joy, peace, patience, kindness, gentleness, and self-control. I dedicate this work and give special thanks to my soul friends Hyosup Kim, Daejoong Kim, and Sungjin Lim for the many years of cheering and putting their warm hearts for me since 1996. Lastly, I thank God for guiding me on this journey with his grace.

Acknowledgements

I would like to take this opportunity to express my deepest gratitude and appreciation to my committee, Dr. Maysam Pournik for tremendous help and patience with me and Dr. Ahmad Jamili and Dr. Ramadan Ahmed for great guidance. Finally, I would like to acknowledge the financial support of the University of Oklahoma, ADNOC, and Petroleum Institute and all the people in Department of Petroleum Engineering in University of Oklahoma are gratefully acknowledged.

Table of Contents

Acknowledgements iv

List of Tables vii

List of Figures viii

Abstract xi

1. Formation Damage Mechanisms 1

    1.1 Introduction 1

    1.2 Surface Deposition 1

    1.3 Mono-Particle Plugging 2

    1.4 Multi-Particle Plugging (Log-jamming) 4

2. Stable Dispersion of Nanoparticles in Aqueous Phase 5

    2.1 Introduction 5

    2.3 Nanoparticles Entrapping Experiments 13

    2.4 Zeta Potential and Particle Size Distributions 16

    2.5 Sandpack Test on Ottawa Sandstone and Indiana Limestone 19

    2.6 Conclusions 21

3. New Insight for Nanoparticle-Based In-Situ Gelled Acid 22

    3.1 History of Acid Diversion Techniques 22

    3.2 Chemical Diversion Techniques 23

    3.3 Advantages of Nanoparticle-Based In-Situ Gelled System 25

4. Propagation of Nanofluid into Indiana Limestone Cores 27

    4.1 Rheology Study of Nanofluid 27

4.2 Coreflood Experiments for Acidizing 30
4.3 Slug Size Design..... 36
4.4 Conclusions 37
5. Surface Modification of Silica Nanoparticles 38
5.1 Introduction 38
5.2 Gelation Tables (Effects of concentration and temperature)..... 39
5.3 pH Sensitivity 42
5.4 Zeta Potential and Mean Aggregate Size 44
5.5 Rheology Studies (Effects of shear rates, concentration of Si and salts) 46
5.6 Breaking Gelation..... 52
5.7 Conclusions 54
6. A Study of Diversion Using Nanoparticle-Based In-Situ Gelled Acids System..... 55
6.1 Sandpack Test..... 55
6.2 Coreflood Experiments for Diversion 63
6.3 Conclusions 74
References 78

List of Tables

Table 4-1. Test conditions for low permeability coreflood experiments 31

Table 4-2. Test conditions for high permeability coreflood experiments 33

Table 5-1 Table 5-1 Gelation Table for room temperature, X: no gel, O : gel, Δ : gel after 24hr 40

Table 5-2 Gelation Table for 90°C……..41

Table 5-3. pH sensitivity of 1.25 vol% Si in different salts 42

Table 5-4. Gelation table with Si + $MgCl_2$..... 48

Table 6-1. Sandpack tests with different nanofluid formulations 58

Table 6-2. Sandpack tests with different flow rates 59

Table 6-3. Single coreflood tests 64

Table 6-4. Mineralogy of Field Core 68

Table 6-5. Single coreflood tests 69

Table 6-6. Calculated shear rates for low and high perm cores 74

List of Figures

Figure 2-1. The scheme of silica 6

Figure 2-2. The scheme of relationship between distance from surface and electrical double layer in colloidal suspensions 8

Figure 2-3. pH-dependence of surface charge of alumina and silica 9

Figure 2-4. Effect of adding salts in nanoparticle dispersion (pH 7) 10

Figure 2-5. Effect of adding a chelating agent in nanoparticle dispersion 11

Figure 2-6. Coreflood apparatus 13

Figure 2-7. Permeability impairment by nanofluid injection 15

Figure 2-8. Particle size distributions and zeta potential measurements for influent and effluent samples 17

Figure 2-9. Size of nanoparticles (aggregates) from TEM, 0.01 vol% silica 18

Figure 2-10. Size of nanoparticles (aggregates) from TEM, 0.01 vol% alumina 19

Figure 2-11. Adsorption of silica and alumina on different rock surfaces 20

Figure 4-1. 2.5 vol% silica/alumina gelation at different pH 27

Figure 4-2. 1.5/1.75 vol%silica/alumina gelation with crushed Indiana limestone 28

Figure 4-3. 1/1.25 vol% silica/alumina gelation with crushed Indiana limestone 28

Figure 4-4. Viscosity comparison 0.75 vol% silica/alumina gelation with crushed Indiana limestone 29

Figure 4-5. Coreflood apparatus 31

Figure 4-6. Pressure profiles and images of core faces (low perm) 32

Figure 4-7. Pressure profiles and images of core faces (high perm) 34

Figure 5-1. 1.25 vol% Si+ 9% $MgCl_2$ at different pH..... 43

Figure 5-2. Zeta potential of silica at different pH..... 44

Figure 5-3. Effect of MgCl2 on mean aggregate size 45

Figure 5-5. Fann viscometer..... 47

Figure 5-7. Viscosity of 0.75 vol% Si with different concentration of MgCl2..... 49

Figure 5-8. Viscosity of 1 vol% Si with different concentration of MgCl2..... 50

Figure 5-10. Viscosity of 1.25 vol% Si with different salts 51

Figure 5-12. Gelation in the core..... 53

Figure 6-1. Sandpack test design..... 56

Figure 6-3. Conductivity measurements during Test 5 60

Figure 6-4. Conductivity measurements during Test 6 60

Figure 6-5. Conductivity measurements during Test 7 61

Figure 6-6. Production ratecomparison between high and low perm sandpack during Test P1..... 62

Figure 6-7. Production ratecomparison between high and low perm sandpack during Test P2..... 62

Figure 6-8. Core images for Test S1 andS2 with 15% HCl .Figure 6-10. Core images for Test S5 and S6 with 1.25 vol% Si + 9% MgCl2 + 15% HCl..... 66

Figure 6-11. Core images for Test S7 with 1.25 vol% Si + 9% MgCl2 + 15% HCl 67

Figure 6-12. Parallel coreflood tests..... 68

Figure 6-13. Core images for Test P1 with 15% HCl 70

Figure 6-14. Core images for Test P2 71

Figure 6-15. Core images for Test P3 72

Abstract

In carbonate matrix acidizing treatment, a major challenge for the operations is to divert the injected acid from the main flow regime into a relatively lower permeability zone due to the intrinsic and unique geological and hydrogeological properties of limestones. The acid applied preferentially flows into the highest permeability zones such as vugs, natural fractures, and largest pores, when injection of acid is initiated in a carbonate formation. Thus, one of the common approaches involves applying a strong acid solution (> 10 wt %) to partially dissolve the limestone in a brief period; the so called "matrix acidizing" operations can be executed to significantly improve hydrocarbons production, or serve other purposes such as to stimulate the waste disposal injection wells to increase injectivity.

In this work, an acid-nanoparticles system has been explored to offer as a retarded acid to manipulate injectivity into high permeability zone so that the acid applied can mainly flow into the low permeability zone. The key concept of designing acid-nanoparticles formulations is to successfully create acidic gel in-situ after injecting silica nanoparticles in solution, and the resulting pseudo-solid shear-thinning gels are largely controlled by varying solution pH, particle concentration, and different types of particle and their ratios. In one example, the selected silica nanoparticles were dispersed in deionized water and blended with electrolytes, magnesium chloride, to modify the silica surface. A series of reaction conditions for generating stable gels were investigated and successful gel formation is strongly correlated to solution pH, concentrations of $MgCl_2$ electrolyte and silica particle, and reaction temperatures. Results of silica aggregate size and zeta

potential measurements also revealed the effects of surface modification by Mg^{+2}. Furthermore, single and parallel coreflood tests were implemented to study the transport behaviors of nanoparticle-based acids in porous media. The cores used in the experiments have a permeability range of 2 to 70 md.

The Mg^{+2}-modified silica particles effectively form gels almost instantaneously at volume fractions of SiO2 as low as 0.75 vol% at neutral pH due to aggregation into networks of silica particles. In general, gel strength drastically increases with elevated concentrations of silica and magnesium chloride. The rates of gelation grow substantially with increase of temperature. The net (negative) values of zeta potential of the silica particles enlarge with increasing pH when higher solution pH directly affects the surface of silica with deprotonation of surface silanol groups. In magnesium chloride amended solution, the silica particles develop a zeta potential within favorable window (0~-5 mv) for aggregation, eventually resulting in formation of gel networks. Results of single core pattern flooding reveal that injection of the new nanoparticle-based formulations creates multiple wormholes and flow channels using both low (2 md) and high (70 md) permeability Indiana limestone core plugs. In addition, injection of the same acid formulation is evidently diverted into the lower permeability core in the parallel setup of corefloods (combined low and high perm cores, 2 md and 70 md) experiments. Results of this study offer preliminary evidences that applying this nanoparticle-based stimulation fluid to form gels in situ is capable to successfully divert the acid into the low permeability core leading to generation of the desired multiple wormholes in both low and high permeability cores simultaneously.

Proper acids are commonly used in well stimulation operations by dissolving formation minerals and foreign material such as drilling mud. The dissolution of these solid materials will increase well productivity. Acidizing techniques are divided into three main categories: acid washing, matrix acidizing, and acid fracturing (Williams 1979). Matrix acidizing is defined as the injection of acid into the formation porosity at a pressure below the fracture pressure. It is achieved either by creating a flow path through a damaged zone around the wellbore or by altering the flow pattern in the reservoir.

There are three main chemical factors related to the selection of acid for a particular stimulation such as stoichiometry, equilibrium, and reaction rate (Williams 1979). The molecular ratio between reaction products and reactants is required for the stoichiometry of an acid reaction with reservoir materials (Kalfayan2008). The general reactions between HCl with calcite and dolomite are shown below.

HCl reaction with Calcite:

$$2HCl + CaCO_3 \text{ ---> } CaCl_2 + H_2O + CO_2 \quad (1)$$

HCl reaction with Dolomite:

$$MgCa(CO_3)_2 + 4HCl \text{ ---> } CaCl_2 + MgCl_2 + 2H_2O + 2CO_2 \quad (2)$$

Dissolving power of the acid on the rocks is crucial to quantify the amount of formation material dissolved by an amount of acid. A thermodynamic equilibrium is reached once acid is totally consumed and equilibrium(s) control the precipitation of reaction product

has been fully met. The reaction rate is conveniently measured by the time required for the acid added to react with the formation materials and the physical geometry of the reaction involved, for example, the distance of the acid penetration is also important due to the complexity of acid reactions.

Different types of acids such as mineral acids, organic acids, powdered acid, and retarded acids are used to maximize the efficiency of stimulation (Williams 1979). The 15 wt% hydrochloric acid is relatively cheap and widely used in most of carbonaceous formations and a mixture of hydrochloric-hydrofluoric acid is used in sandstone stimulation as mineral acids. However, high corrosivity is a major issue of using hydrochloric acid especially for the high temperature above 250°F (Williams 1979). Furthermore, aluminum- or chromium-based materials in common pumps have high tendency to be damaged. Organic acids such as acetic acid and formic acid have relatively lower corrosivity which allow the acids to be used in operations requiring a long-acid-pipe contact time and it is also easier to control inhibition at high temperature (Williams 1979). Powdered acids are relatively expensive than hydrochloric acid and their utilization are limited in well stimulation due to the portability to remote locations. In economic perspective, cost per dissolving power increase from acetic to formic acid and from formic to hydrochloric acid (Kalfayan 2008). In order to design appropriate acid type, factors such as mineralogy, temperature, corrosivity, cost, and efficiency of penetration are important. The main focus of this work is designing viable approaches for successful propagation of acid-nanoparticles system in porous medium prepared with stable dispersion of nanoparticles. The acid-nanoparticles system belongs to the

category of retarded acid. Retarded acid system is usually used in oil well acidizing by decreasing reactivity. The decrease of reactivity accompanied by thickening agents or addition of artificial gums effectively assists acid to penetrate deeper in the damaged zone before the acid being spent. For example, the gelled acids are used to retard acid reaction by increasing fluid viscosity which reduces the rate of acid transferred to the zone. For instance, partially hydrolyzed polyacrylamide based polymer can be mixed with a group of zirconium and aluminum salts prepared in formic acid and hydrochloric acid blends to form in-situ-gelled acid (Rabie 2012). The in-situ-gelled system based on hydrochloric acid show the efficient degree of gelation and diversion at a relatively low injection rate (2 ml/min) and it is confirmed by coreflood study, CT scan, and reaction rate measurements. Different acid system has different crosslink properties of the system. Therefore, sufficient understanding of acid-polymer chemistry and physical properties are required to develop in-situ-gelled acid. One of the drawbacks of using gelled acid is that the gelling agents degrade in acid solution at temperature above 130°F and they are not often used in matrix acidizing due to the injectivity loss by the high viscosity. Other types of retarded acids are chemically retarded acids and emulsified acid. Both cases are formulated with surface active agents or polymers. The chemically retarded acids are typically comprised a mixture of oil-wetting surfactant and acid capable to build a physical barrier between acid and the rock surface. In order to form a coherent film on the rock surface, some functional additives must first adsorb on the rock and the acid should be injected continuously during the treatment. The cons of using this system are the ineffectiveness when adsorption is diminished at high flow rates and high formation temperatures. Alternatively, the emulsified acid systemconsist

of dual oil and aqueous phases. Oil is usually the external phase and acid is the internal phase. The pre-emulsification step increases the fluid viscosity and the external oil layer can effectively retard the rate of acid transferred to the rock offering deeper penetration of acid. Emulsified acid was also used in acid fracturing for high temperature carbonate reservoir (Navarrete 1999). In matrix acidizing, the effect of oil saturation is significant and it is confimed that 2 to 2.5 times of the emulsified acid volume is needed to stimulate the same well if there is no oil in the vicinity of wellbore (Sayed 2014). An empirical wormholing criterion for acids is developed based on the rheological behavior by power law and the criterion can be used to estimate optimum injection rate for different types of carbonate formations (Maheshwari 2015). The stability of emusion acid fluid is closely related to acid droplet size and temperature. Coreflood study show that polymer-assisted emulsified acid enhance diversion capability (Zakaria 2015).

In this endeavor the retarded acid system, the selected fumed metal oxide nanoparticles are used to build up viscosity. The fundamental concept of creating gelation is that hydroxyl groups on the surface of the nanoparticles react with water molecules in aqueous solutions as documented in a previous paper of this group (Weston et al. 2014). It produces charged surface species and their magnitude and sign of surface charge strongly rely on solution pH. The binary silica and alumina oxide mixtures show strong interparticle interactions when one is positively charged and another is negatively charged between the isoelectric points of silica and alumina. Once the mixtures are at a desired pH, it forms pseudo-solid gels. The gelation region of the mixtures is between pH 4 and pH 8 with 1.75 vol% of the total nanoparticles (Weston et al. 2014). It also

shows the dependence of total volume fraction on gel properties. As total volume fraction increases, the gel strength increases. There are several ways to break the gelation such as changing solution pH, increasing temperature, and applying intensive shear rate. When pH is changed to higher than pH 8 or lower than pH 4, net charge of the particles changes and surface of the metal oxide nanoparticles is deprotonated (> pH 8) or protonated (< pH 4) . Therefore, the interparticle forces become weaken dramatically and the gel breaks, eventually. This system involves pseudo-solid shear thinning and temperature sensitive species. The effects of sodium chloride, calcium chloride, and magnesium chloride are tested in a series of experimental works and different techniques of sample preparation are explored to maximize the stability of nanoparticles dispersion in extreme harsh solution conditions.

The effect of different ions such as sodium, chlorine on particle dispersion was studied decade ago (Tombacz et al. 1996). The various ions distinctly affect the electrostatic interaction which is the main driving force to form gel. The rheological properties of the fumed nanoparticles are studied (Cerbelaud et al. 2008). The fractal structures of nanoparticles can create multi-dimensional rigidity and it cause less dense aggregates formation.

Once stable dispersion of these nanoparticles was established, further coreflood experiments were conducted to understand how these nanoparticles propagate through the Indiana limestone core samples. Three possible mechanisms of formation damage were introduced and monitored. Screening (Mono-Particle Plugging) is the physical entrapment of nanoparticles in pore throats where the size of nanoparticle are much

bigger than the pore throat to pass. (Civan 2007) shows that for pore throat to particle size ratios between 7 and 3, pore plugging and internal filter cake may occur. Log jamming is the physical entrapment of clusters of smaller nanoparticles when the nanoparticles are accelerated through a narrow pore throat, the nanoparticles accumulate into clusters that are larger than the sizes of throats (Skauge, Spildo, and Skauge 2010). Surface deposition is the retention of the particles by physicochemical forces due to electrochemical interaction between the nanoparticles and rock surface. After permeability impairment coreflood experiments, the nanoparticles were also mixed with hydrochloric acid and injected though Indiana limestone cores to confirm the satisfactory propagation of nanoparticles with the pre-existing wormholes in the core matrix.

1. Formation Damage Mechanisms

1.1 Introduction

Understanding nanoparticle's fate and transport phenomena through porous media is another critical concern. There are several mechanisms and forces that determine whether nanoparticles will transport or be trapped in the porous media. Although some suggested that nanopartilces will flow easily through porous media due to their tiny size, more recent data showed that nanoparticles can potentially cause suddent permeability impairments (Alaskar et al. 2012, Hendraningrat et al. 2012, Skauge et al. 2010, Yu et al. 2012). Based on these, there are at least three main mechanisms that can cause particles entrapment (retention): surface deposition, pore throat clogging (i.e., mono-particle plugging) and log-jamming (i.e., multi-particle plugging).

1.2 Surface Deposition

Herzig et al. (1970) demonstrated that for the suspension of tiny particles (size less than 100 nm) that flow through porous media, the main retention forces are physicochemical forces (van der Waals attractive force and electrokinetic force). They further described that the main transport mechanisms of the particles to the retention sites on the grain surface were direct interception and diffusion. Alaskar et al. (2012) showed that surface adsorption is due to electrochemical interactions between the nanoparticles and the surfaces of rock. Their work investigated the effect of surface charge (of particles) and the shape of particles on particle retention in the Berea core samples. They found that when particles with a surface charge opposite of the porous media were injected they

were not able to travel far in the core sample, this indicated that strong electrical attraction dominated and the particles were adsorbed to the oppositively charged grain surfaces. It was also determined that besides surface charge, particle geometry plays a significant role in its ability to navigate through pore spaces. The work of Gruesbeck and Collins (1982a) suggested that there existed a critical seepage velocity that was closely associated with the high shear stress against particles previously sorbed on to the grain surface, eventually caused them to be released from the soprtive sites. They argued that when the shear stress of hydrodynamic forces exceeded this critical shear stress, the sorbed particles would release from the surface. Civan (2007) also described that the critical shear stress can be interpretated as a function of the adhesion of the particles to the surface of the rock. In the same work, the author provided some correlations to estimate the critical shear stress for particle detachment.

1.3 Mono-Particle Plugging

The behavior of mono-particle plugging (or Screening mechanism) can be simply described as the physical entrapment of large nanoparticles approaching pore throats that are too tiny to allow physical passage. Hendraningrat and Torsæter (2014) reported that nanoparticles can easily agglomerate after dispersed in water as they are fully hydrated and equilibration. Since nanoparticles exhibits quite large specific surface area to volume ratios, and high surface energy to disperse, they will tend to agglomerate in bulk to reduce the surface energy. The suspended aggregates in solution can grow to few hundreds nanometers in size which may be sufficient big to plug smaller pores in

the media. Hendraningrat et al. (2012) investigated the effect of specific surface area on particle retention, and they concluded that under similar injection rate and same concentration profiles of particles, the particles selected with two different surface areas would yield different permeability impairment results. They observed that the dispersed nanoparticles with lower specific surface area showed significant less amount of retention and consequentially smaller permeability reductions. Civan (2007) showed that for pore throat to particle size ratios ranging from 3 to 7, pore plugging and internal filter cake can occur. Gruesbeck and Collins (1982b) studied the migration of particle suspensions through perforations. They concluded that the maximum particle concentration that can successfully flow through the perforations without severe plugging largely depends on the ratios of the perforation diameter to the particle diameter. Chang and Civan (1991) used a bimodal function to model the effect of pore size distribution and particle size distribution on permeability impairment due to particulate transport in porous media. Mustin and Stoeber (2010) discussed that the predominant filtering mechanism for large particles is size exclusion, meaning large particles are trapped as a result of size exclusion by relatively small pore throats. They also discussed the importance of knowing particle size distribution as they clearly demonstrated that polydisperse nanoparticle solutions caused greater permeability reduction after core flooding than monodisperse samples. They concluded that the larger particles would clog the majority of pore throats and the smaller particles would then come behind and completely fill in the smaller gaps resulting in more severe damages than a monodisperse system involving only relatively large particles.

1.4 Multi-Particle Plugging (Log-jamming)

The Log-jamming mechanism as discussed by Skauge et al. (2010) is the physical entrapment of clusters of relatively smaller nanoparticles which mainly cause by the distinct weight differences between the heavier nanoparticles and the particle carriers, much lighter solvent molecules. When these two components are travelling side by side approaching the narrow pore throats, the dense nanoparticles experienced the lagging effects and accumulated into clusters that are significantly larger than the throats they are attempting to navigate. Excessive lagging behavior likely leads to complete pore throat blocking and severe permeability damage which is sometimes irreversible. Civan (2007) pointed out the key controlling factors of the log-jamming includes the particle Reynolds number and the pore throat to particle diameters ratio. Increase of particle velocity results in larger Reynolds number and largely increase the possibility of jamming to occur. Rodriguez Pin et al. (2009) showed that injecting high concentrations and elevated injection rates of nanoparticle solutions will generally cause more intensive permeability impairments. This is largely in agreement with others' observations that increasing nanoparticles concentrations will have larger numbers of nanoparticles per unit volume to cause permeability impairments due to multiple mechanisms invloving size exclusion, surface adsorption, or log jamming. The effect of the injection rate and the higher particle velocities experienced could cause the lagging effect becoming dominated.

2. Formulating Stable Dispersion of Nanoparticles in Aqueous Phase

2.1 Introduction

One of the important considerations of successful nanofluid applications in porous media is the stability of particle dispersion. Nanoparticles possess a charged surface (e.g., silica has negatively charged surface and alumina, instead, has positively charged at neutral pH 7), thus the dispersed particles can be adversely affected by adding the oppositely charged ions either in the solution or on the matrix rock surface. Chang and Vigneswaran (1990) reported that in general as the salinity of the dispersed fluid increases the amount of particles deposited on the surface of porous media increases. They further explained that increase of salinity causes the repulsive double layer force to be suppressed, which allows attractive forces to dominate causing adsorption to occur. Ghadimi et al. (2011) documented that a stable nanofluid at high salinity can be achieved through surface charge density manipulation either by particle surface modifications, controlling ionic environment of the fluid via surfactants, or a combination of both. Others (McElfresh et al. 2012) found that nanofluid dispersion could become quite unstable downhole when met harsh salinity or temperature conditions. They were able to achieve stable dispersion at the adverse conditions by surface modification of the nanoparticles, i.e., adding stabilizers to the solution and modifying solution pH.

The aim of this study focused specifically on having better understanding of various nanoparticles damage behaviors in carbonate media at different conditions of flow rate, nanoparticle type and concentration, which affect designing solid-based acidizing formulations. A series of bench-scale experiments were conducted to mimic flow-through condition of acidizing operation, and the results were simulated using Wojtanowicz et al.

(1987, 1988) models for assessing the possible damage mechanisms created by injecting nanoparticles. In addition, a dimensional analysis was further applied to correlate the most important parameters that control nanofluid migration through the core samples. Particle size distribution and presence of sedimentation are the criteria to check the stability of nanoparticles in solution. When the nanoparticles are stable, the particles are in Brownian or colloidal stabilization so that the particles can be suspended in the solution. The surface of silica particles hydrates to form silanol groups (Si-OH). For example, silanol groups react with OH^- and ionized then produce SiO^- groups on the surface (Karami 2009). Since the particles are negatively charged, an electrical double layer is formed with ions of opposite charge as shown in Fig 2-1. This electrical double layer plays an important role in stability of the colloidal dispersion.

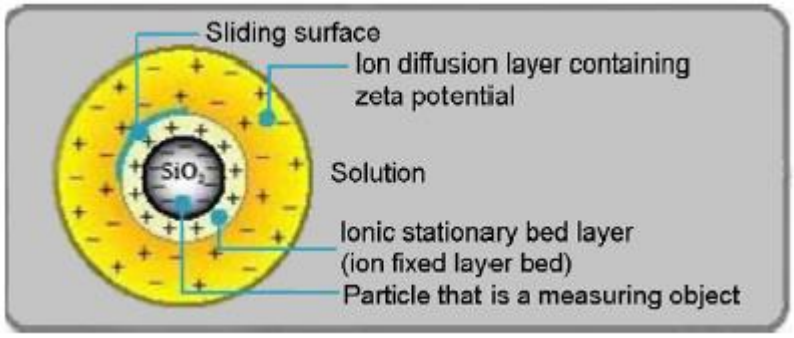
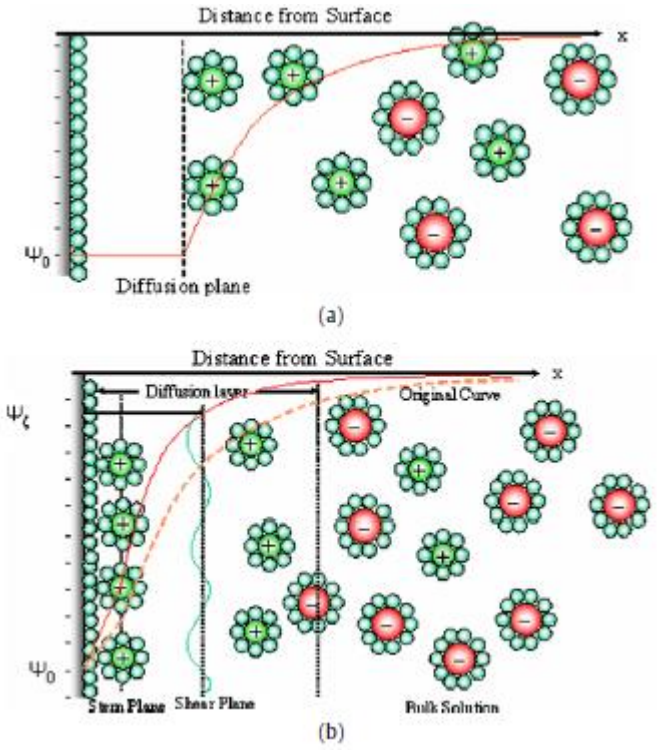


Fig 2-1. The scheme of silica (Karami 2009)

The surface potential of silica decays exponentially with distance way from shear plane in Fig 2-2a. The higher salt ionic concentration, the faster the decay causing the double layer shrinks because it is a function of free salt ionic concentration (Karami 2009). By adding salt on the system, the value of surface potential does not change but stern

potential changes and the sum of surface and stern potential is a crucial factor in stability. When high concentration of salt introduced on the system, stern potential becomes zero and double layer collapses then van der Waals forces dominate over repulsion by increasing the probability of interparticle collision (Mazzone, Tardos, and Pfeffer 1986). This eventually leads to aggregation and gelation which is a phenomenon called “salting out” effect as shown in Fig 2-2c.



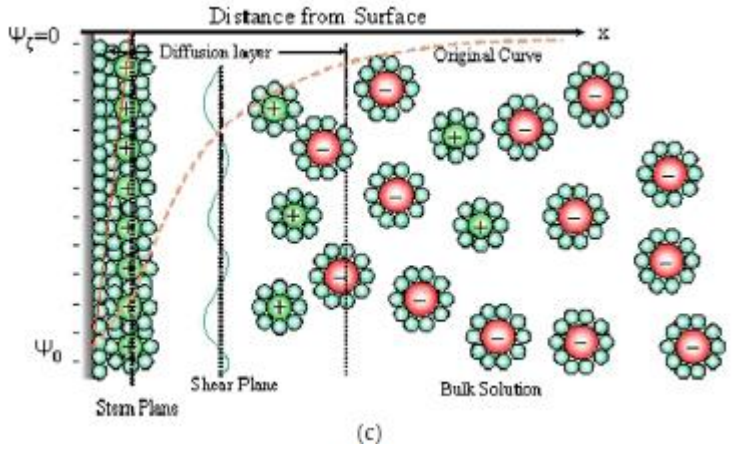


Fig 2-2. The scheme of relationship between distance from surface and electrical double layer in colloidal suspensions (Karami 2009)

The main difference between silica and alumina particles is surface charge. The point of zero charge for silica is about 4 and for alumina is 8 (Sulman 2010). As shown in Fig 2-3, the surface changes with pH. For instance, alumina is positively charged and silica is negatively charged at pH 7. Therefore, there is high probability of gelation, when silica and alumina is mixed at pH 7. The ratio between silica and alumina can also shift the gelation region.

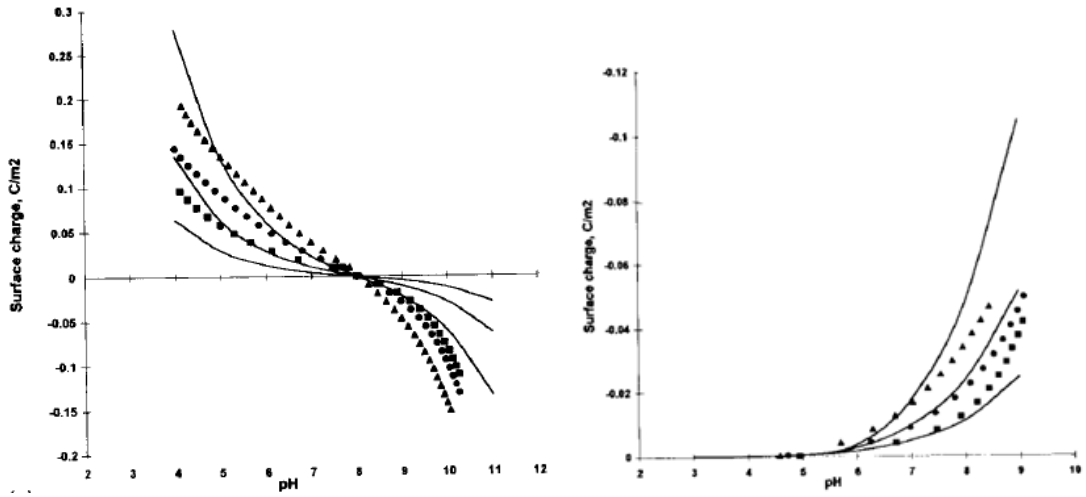


Fig 2-3. pH-dependence of surface charge of (left)alumina and (right) silica (Tombacz et al. 1996)

2.2 Phase Behavior Test

Two fumed metal oxide nanoparticles are selected based on their commonly used in areas such as pigments, viscosity adjusters, catalyst supports, and fillers. Both silica nanoparticles (primary diameter of 7nm) and alumna (diameter of 13nm) were purchased from Evonik (Essen, Germany) came as powder form (Bobe 2006). The fumed silica and alumina nanoparticles were selected due to their stable dispersion in aqueous phase and high grade purity (Weston 2014). The common manufacturing process is described as the continuous flame hydrolysis of silicon tetrachloride ($SiCl_4$). In this process, raw $SiCl_4$ is thermally converted to gas phase and then reacts spontaneously in an oxyhydrogen flame with the intermediately-formed water molecules to achieve the desired product of silicon dioxide and alumina oxide. The nanoparticles were manufactured by flame pyrolysis at high temperature (1000 °C). During the pyrolysis process, the molten, spherical primary particles collide with one another and form fractal aggregates. In this work, for

preparation, deionized water (DI) was used and an ultrasonic dismemberator (Fisher Scientific F505) equipped with a CL-334 Converter was used as a sonication device for homogenization. The Indiana limestone core plugs (purchased from Kocurek industries, TX) were cut out of 7" cube into individual 1.5" x 6" cylindrical plugs and have average porosity of 16% with initial permeability of 8~10 md. .

The stability of silica and alumina was individually tested in laboratory experiments. Firstly, nanoparticles were mixed with deionized water and a horn sonication was used for 20 minutes with 20% amplitude. First two samples in Fig 2-4 shows stable dispersion for both 0.5 vol% silica and alumina. However, severe sedimentation was observed after adding 1% NaCl on the right side in Fig 2-4.

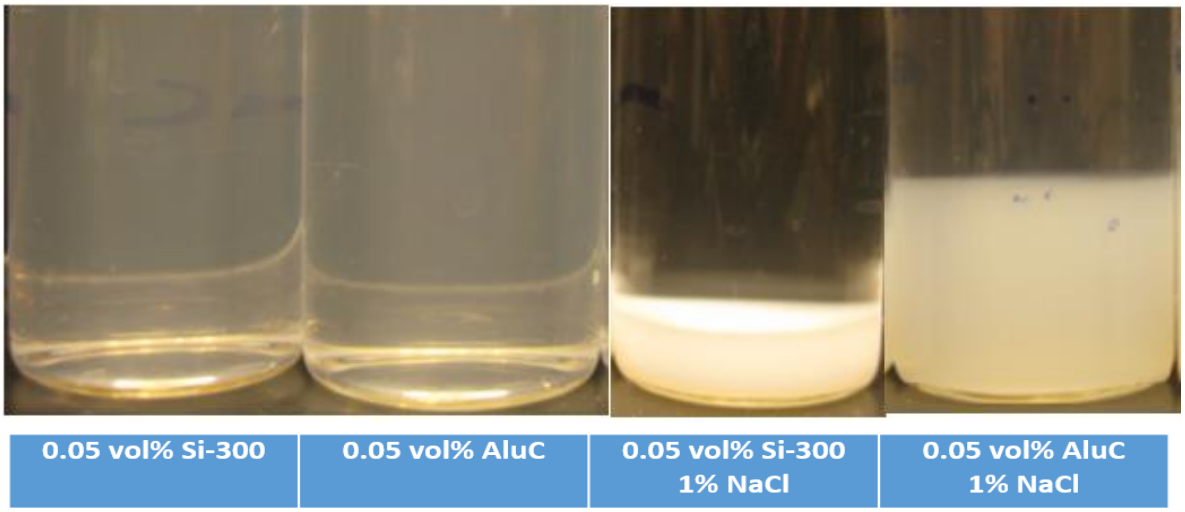
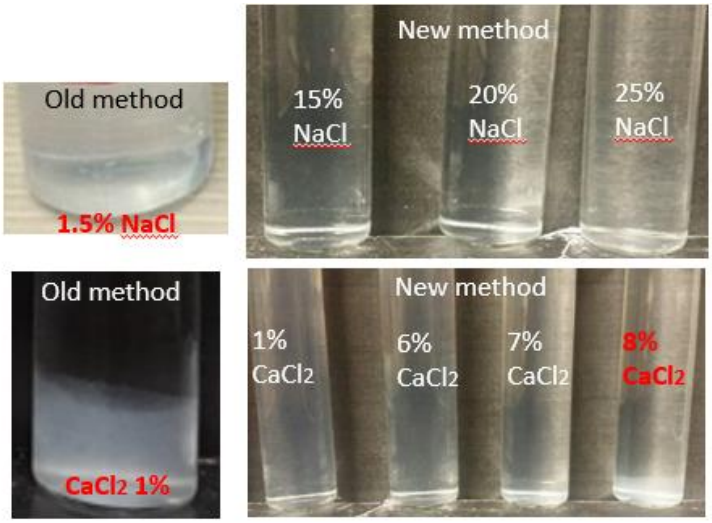


Fig 2-4. Effect of adding salts in nanoparticle dispersion (pH 7)

The electric double layer of the nanoparticles is compressed as sodium chloride is added and change the electrostatic interaction between the particles. Therefore, the

nanoparticles can form large aggregates causing particles settled down due to gravity. When solid particles are immersed in a liquid, it often remains attached in the form of clumps and those particles that do disperse in the liquid clump together again to form larger aggregates that settle out of the suspension. Even with the dispersion of particles, the dispersion may be viscous or thin. The particles may remain dispersed for different lengths of time, and the dispersion to molecular environment is sensitive to pH, temperature, additives (Rosen 2004).



	Old Method			New Method (w/ CA)		
	NaCl (%)	MgCl (%)	CaCl2 (%)	NaCl (%)	MgCl (%)	CaCl2 (%)
0.03 vol% AluC	0.3	N/A	0.1	0.3	0.1	0.1
0.03 vol% Si-300	1	N/A	0.5	25	0.7	7

Fig 2-5. Effect of adding a chelating agent in nanoparticle dispersion

In order to reduce the reactivity of the salts in solution, a chelating agent with three carboxyl groups was introduced. The overall salt tolerance of nanoparticle dispersion is improved significantly as shown in Fig 2-5 and it is confirmed that there are more uniform particle size distributions by adding the chelating agent. In acidic conditions, the pH of the aqueous phase is lowered. The surface of nanoparticles become increasing positive or less negative, since protons from the solution adsorb onto the charged sites. For example, silica particle formation and growth in extreme low (or negative) pH solutions happens when monosilicic acid disappears by a second order dimerization reaction and mean floc diameter increases exponentially in time as primary particles flocculate (Gorrepati et al. 2010). Polymerization was used to increase repulsive force between the nanoparticles.

Nanoparticles have a surface charge so it can be adversely affected by oppositely charged ions either in the solution or on the rock surface. Chang and Vigneswaran (1990 determined that in general as the salinity of the dispersing fluid increases the amount of particles deposited on the surface of porous media increases. They mentioned that the increase in salinity causes the repulsive double layer force to be suppressed, which allows attractive forces to dominate causing adsorption to occur. Ghadimi et al. (2011) demonstrated that nanofluid stability at high salinity can be achieved through surface charge density manipulation either by particle surface modification, control of the ionic environment of the fluid via surfactants, or a combination of both. McElfresh et al. (2012) found that nanoparticle dispersion becomes unstable downhole at harsh conditions of salinity or temperature. They

were able to get a stable dispersion at these conditions by surface modification of the nanoparticles, introducing additives to the solution and /or pH modification. In acidic conditions, polymerization of silica was effective and short-range repulsive force is needed to distinguish between hydration force silica hairs for polymerization (Gorrepati et al. 2010).

2.3 Nanoparticles Entrapping Experiments

Indiana limestone core plugs were first oven dried overnight at 200°F and saturated with DI. Then the cores were weighted and porosity was calculated based on the difference between dry and wet cores. This difference in weight can be then used to calculate the porosity using the formula:

$$Porosity\ \% = \frac{\frac{Wet\ weight - Dry\ weight}{Density\ of\ DI}}{Bulk\ volume}\ x\ 100$$

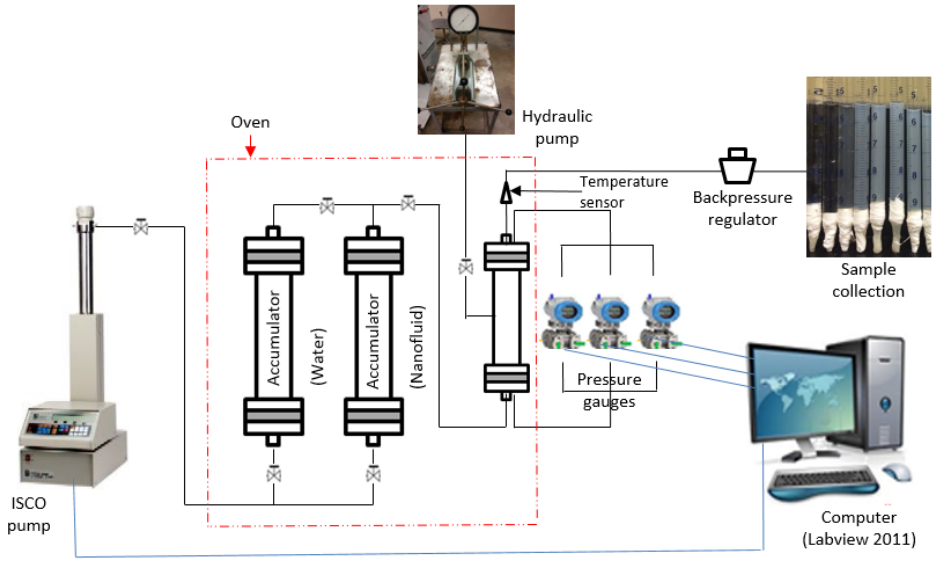


Fig 2-6. Coreflood apparatus

Figure 2-6 depicted the set up of coreflood apparatus. Intrinsic fluid (water) permeability was calculated by differential pressure between inlet and outlet of core using the Darcy's law using multiple flow rate tests,

$$k = \frac{q\ \mu\ dL}{A\ dP}$$

Conversion factor is introduced to express in proper units in coreflood tests as following:

$$k = 122.78\frac{q\ \mu\ dL}{D^2\ dP}$$

Where

k = Permeability of the core in mD

D = Diameter of the core in inches

μ = Fluid viscosity in cp

dL = Length of the core in inches

dP = Pressure drop across the core in psi

Coreflood experiments were conducted by injecting various concentrations (0.01~0.5 vol%) and injection rates (0.3~3.5 ml/min) in order to analyze different formation damage mechanisms such as gradual pore blocking, screening, and straining. All coreflood experiments were run at room temperature (23 °C) and maintained a confining pressure of 500psi. Differential pressure between the inlet and outlet of cores was monitored with a PC installed with a Labview 2011 sofeware and any permeability

changes were calculated based on the water permeability measured in pre-saturation stage prior to nanofluid injection. Permeability change at different flow rates and the concentrations of nanoparticle used are shown in Fig. 2-7. The permeability changes were obtained from the ratios between differential pressure during the injection of nanofluid and the pre-water flooding. Both alumina and silica particles were tested with different flow rates and concentrations in order to reveal the impacts of different mechanism. As the concentration of alumina or flow rate increases, there is sharp transition of mechanism from gradual pore blocking to straining (Fig. 2-7). Higher concentration of silica (0.03 vol%) causes damage shifting from screening to straining by high mass transport rate. Higher injecting rate also causes severe damage shifting from screening to mostly straining after the injection of 5PV.

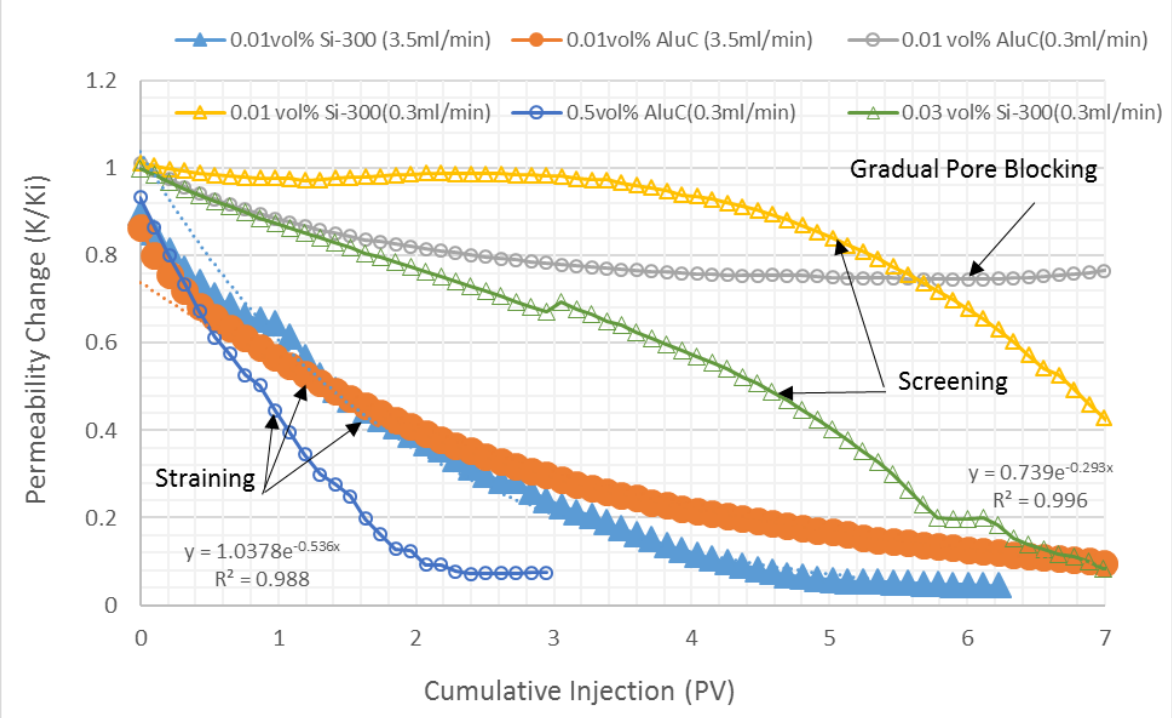
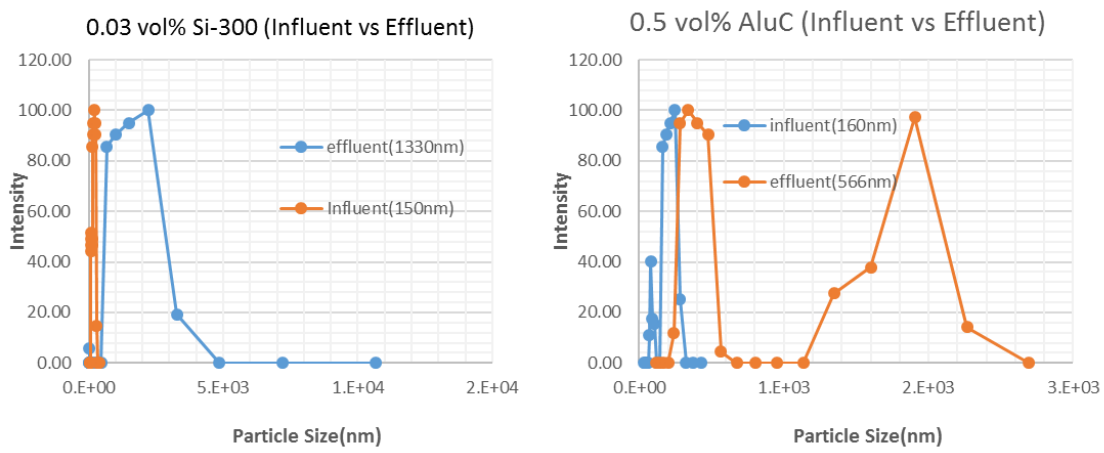


Fig 2-7. Permeability impairment by nanofluid injection

Permeability impairment at different flow rates and the concentrations of nanoparticle is shown in Fig 2-7. The permeability data was obtained from the ratio between differential pressure during the injection of nanofluids and the preflush of water. As the concentration of alumina flow rate increases, there is the transition of mechanism from gradual pore blocking to straining. Higher concentration of silica causes severe damage shifting from screening to straining since higher concentrations of nanoparticles have a greater amount of nanoparticles per unit volume to cause permeability impairments. Numerous works (Alaskar et al. 2012; Hendraningrat et al. 2012; Skauge et al. 2010; Wojtanowicz et al. 1987; Yu et al. 2012, to name a few) also showed that propagation nanoparticles can cause permeability impairment. The main retention forces are van der Waals and electrokinetic forces and direct diffusion and interception cause nanoparticle retention on the rock surface (Herzig et al. 1970).

2.4 Zeta Potential and Particle Size Distributions

The size distributions were quantified by the DLS measurement (ZetaPALS, Brookhaven Instruments) for aqueous suspension plus the TEM analysis (JEOL 2000-FX) was conducted separately as a supplemental tool for size distribution analyses. The effective diameters for both silica and alumina are rather close regardless of the concentration of particles.



	0.01 vol% Si-300 (Influent)	0.03 vol% Si-300 (Influent)	0.01 vol% AluC (Influent)	0.5 vol% AluC (Influent)	0.03 vol% Si-300 (Effluent)	0.01 vol% AluC (Effluent)	0.5 vol% AluC (Effluent)	DI water (Effluent)
Zeta Potential (mv)	-40	-47	65	59	-14	-5	-12	-14
Effective Diameter (nm)	145	150	165	160	1330	750	566	1940

Fig 2-8. Particle size distributions and zeta potential measurements for influent and effluent samples

In general, the resulted aggregate size is dependent on inter-particle forces corresponding to the charge density of particle surfaces. The large aggregation size is expected when approaching the isoelectric points for mixtures or increasing nanoparticles concentrations. The surface charge of these two nanoparticles investigated depends on the pH values, mainly by deprotonation or protonation of hydroxyl groups located on the surface of the metal oxide nanoparticles. Therefore, larger aggregation size is expected while approaching at the point of zero charge (PZC) for individual nanoparticles.

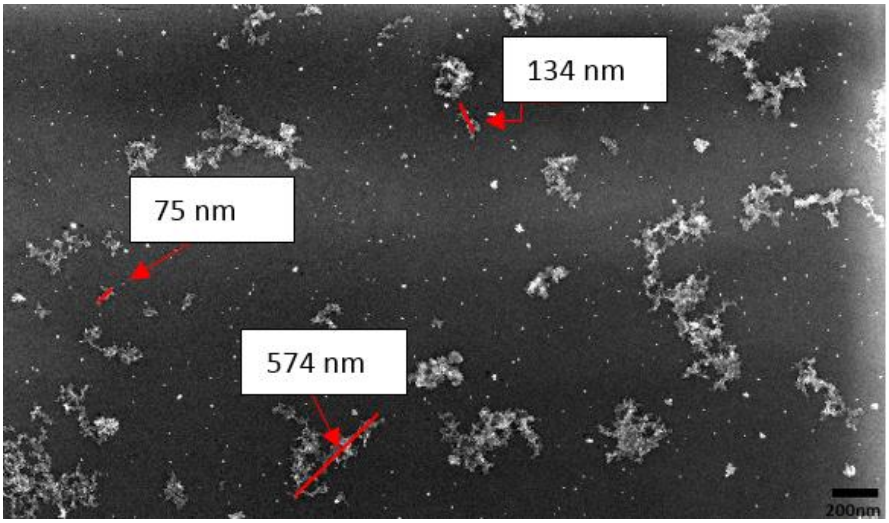


Fig 2-9. Size of nanoparticles (aggregates) from TEM, 0.01 vol% silica

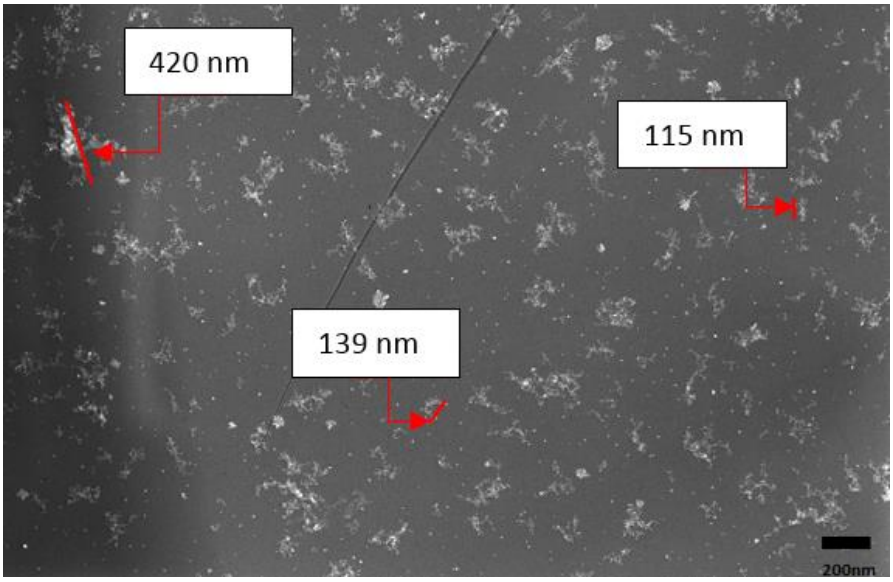


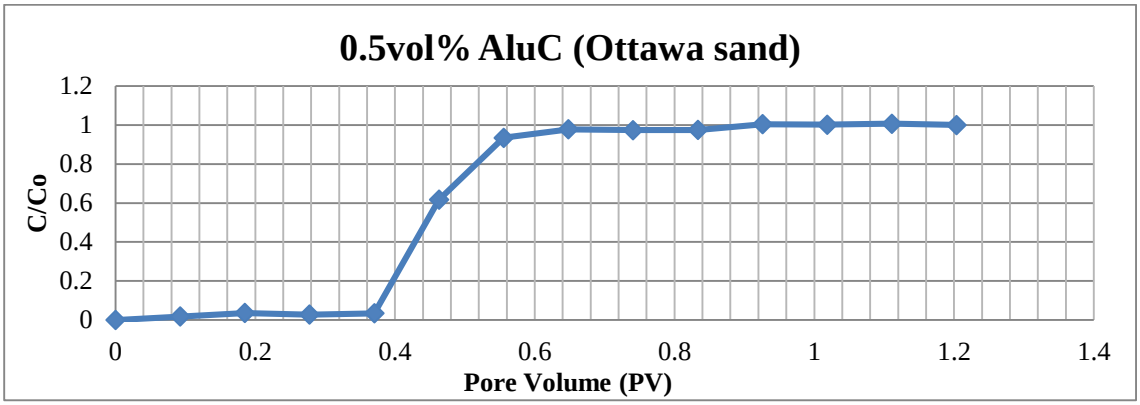
Fig 2-10. Size of nanoparticles (aggregates) from TEM, 0.01 vol% alumina

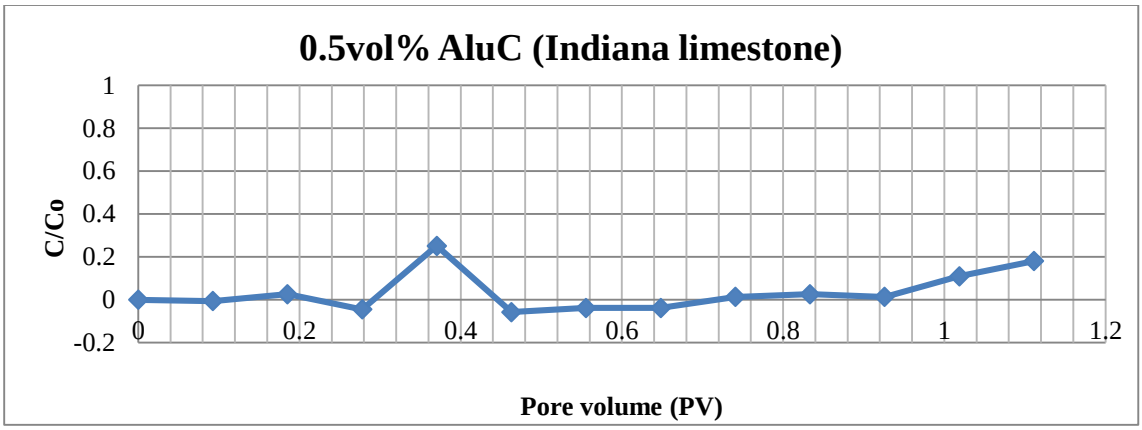
The TEM images shown in Figures 2-9 and 2-10 are the observed fractal shaped aggregates for silica and alumina in this effort. Based on the TEM data and an image software package (ImageJ), the average aggregate size was estimated for Alumina (256 ± 62 nm) which has relatively uniform size distribution than silica (230 ± 135nm). These

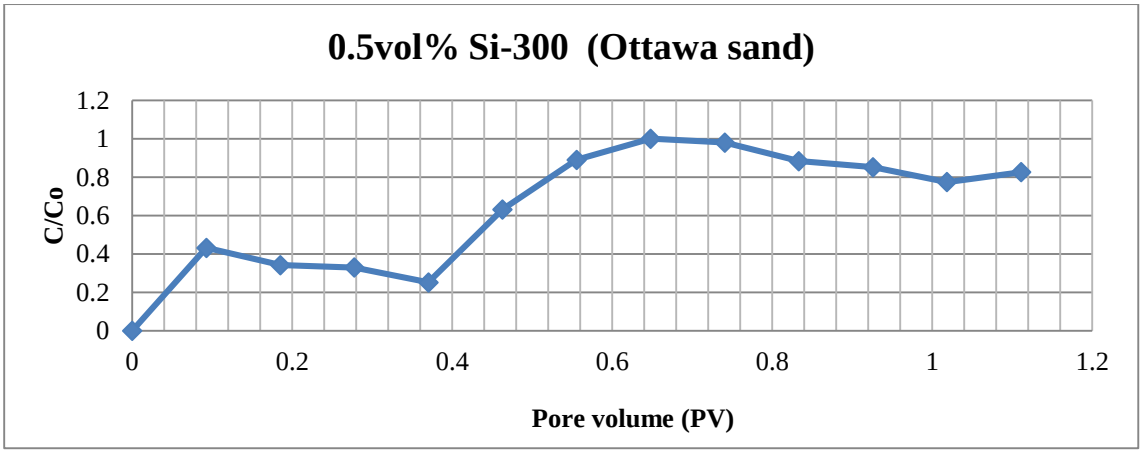
results may reveal that alumina are capable of attaching more to the grain particles because of the +3 charged surface, which means higher attraction forces, and the aggregates should have larger diameter than silica which has instead a -2 charged surface. This corresponds with the size distribution from the DLS data showing silica has wider range in sizes at 0.01 vol%. Similarly, mean size distribution of fumed silica reported around 226nm by DLS previously (Mora-Barrantes 2011).

2.5 Sandpack Test on Ottawa Sandstone and Indiana Limestone

A series of sand pack tests was implemented in vertical orientation to simulate one dimensional reservoir flow. The porosity (33%) of crushed Ottawa sandstone and Indiana limestone was measure by a 50 mL volumetric cylinder and the same grain size was used after sieving.







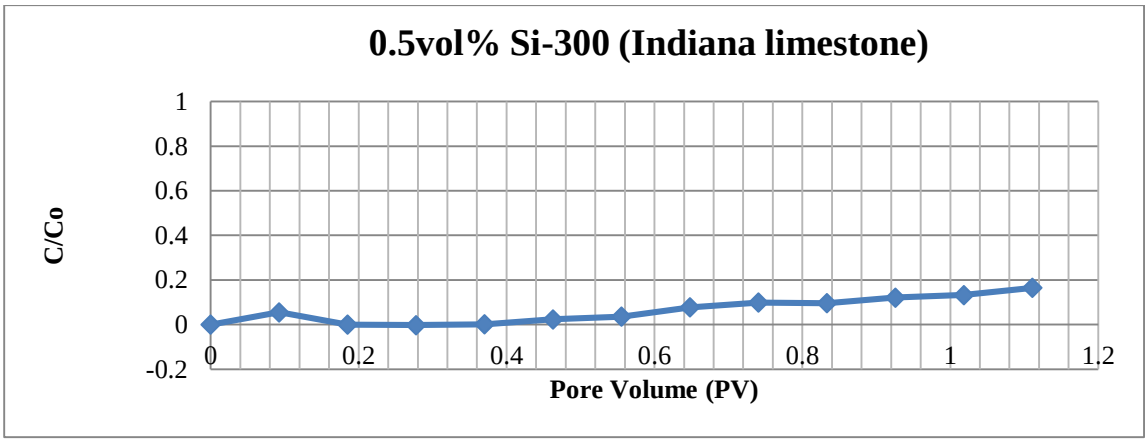


Fig 2-11. Adsorption of silica and alumina on different rock surfaces

The apparatus is Kontes chromatography column with 1 inch in diameter and 6 inches in length. The fluids were injected from the bottom and through a flow adaptor. The column was pre-saturated with deionized water and nanofluid was injected. Effluent samples were collected every 0.09 pore volume and analyzed by UV-vis to detect concentrations of nanoparticles in the samples. Fig 2-11 shows that there is more severe adsorption on Indiana limestone than Ottawa sandstone for silica and alumina. Alaskar et al. (2012) studied the effect of surface charge and particle shape on particle retention in a Berea sandstone core sample. When oppositely charged particles are injected into porous medium, electrical attraction dominates and the particles are adsorbed on the surface of the rock. Since Berea snastone has opposite net surface charge compared to Indiana limestone, nanoparticles are more adsorbed on Berea sandstone than Indiana limestone. In order to prevent the adsorption on Indian limestone, surface coating for nanoparticles or preflush with additives is required to flip the surface charge of Indiana limestone. Civan (2007) also investigated the role of critical shear stress for the adhesion of nanoparticles on the surface of the rock. However, applying high shear stress to release adsorbed nanoparticles seems not pratical in field applications since matrix acidizng should be performed below fracture pressure.

2.6 Conclusions

- Stable dispersion of nanoparticles is desired to minimize damage in the cores. Salt tolerence of nanofluid disperion needs to be further improved since there is severe sedimentation by adding 1 wt% sodium chloride.

- Average pore size (152~168 nm) of Inidiana limestone core was not big enough to avoid pore bocking by nanoparticles (53~574 nm for silica and 46~420 nm for alumina) .
- Different mechanisms for the mechanical entrapping of nanopartidcles were observed from coreflood tests. The higer comcentration of nanoparticles (0.03 vol% of silica and 0.5 vol% of AluC compared to 0.01 vol%) and the faster flow rate (3.5 ml/min compared to 0.03 ml/min) cause more severe damage such as straining or log jamming.
- More surface depostion of silica (negatively charged) is speculated due to the oppositely chareged Indiana limestone surface (positivelycharged) at neutral pH. Further study on electrokinetics between nanoparticles and Indiana limestone is required to quantify surface depostion of nanoparticles.

3. New Insight for Nanoparticle-Based In-Situ Gelled Acid

3.1 History of Acid Diversion Techniques

There are two main technical approaches to create effective diversion of the acid, mechanical-diversion and chemical-based diversion. For example, installation of opposed cup packers, squeeze packers, coiled tubing, and ball sealers are commonly used mechanical diversion techniques. These techniques have intrinsic uncertainty and limitations. For example, use of coiled tubing has an ability to attach the injection nozzles to reach certain zone in wells that exhibit high water production rates. However, adoption of smaller diameter nozzles causes much higher friction losses and increasing

pressure which inevitably reduces the injection rate. Solid-form particulate diverters or ball sealers are very difficult to evenly distribute in the coiled tubing. To use ball sealers in diversion, the selected small balls are first pumped into wells along with stimulation fluids to properly seat the ball on perforations to form a temporary seal. However, it has been argued that this is not effective in cased and perforated horizontal wells due to difficulties in seating the balls at the perforations along the top side of the pipe (Kalfayan 2009). Installation of downhole packers can be used to prevent fluid flow at the end of tubing to direct fluids into intervals with minimum or no flow. However, this is expensive and only guarantees fluid entry into a single interval; to treat multiple intervals requires repositioning of the packers after each acid treatment.

3.2 Chemical Diversion Techniques

Injection of organic acids, gelled acid, in-situ gelled acid, emulsified acid, and viscoelastic acid are among the main choices for chemical-based diversion. Organic acids such as acetic acid and formic acid are used due to their lower corrosivity and the relative ease with which their corrosivity can be passivated at high temperatures. Based on the cost of acid per unit, associated with dissolving power, organic acids are more expensive than hydrochloric acid. They also have lower viscosity which is unfavorable for treating large permeability contrast ratios in multilayered zones. The in-situ gelled acid technique involves injecting multiple compounds, including polymer (a gelling material used to increase the viscosty of of the acid), the crosslinkers (e.g. ferric chloride, where the Fe^{+3} ions are used in crosslinking the individual polymer chains at pH 2, which significantly increases fluid viscosity), the breaker (e.g., sodium

erythorbate used to reduce the ferric ions to ferrous (Fe^{+2}) ions, reducing the viscosity gain caused by the presence of ferric ions), corrosion inhibitor and buffer (hydroxyacetic acid), which initiates polymer degradation and whose active ligand removes the metal ions from the polymer to allow further degaration of the polymer gel, in turn reducing the viscosity (Nasr El Din 2011). Data also show that the in-situ gelled acid system tends to exhibit the plugging issues that were inherent with the conventional cross-linked acid gellants (Woo, 1999). Chang et al. (2001) noticed that in-situ gelled acid caused a loss in the permeability in tight carbonate cores because of polymer-gel retention at the core face. Gomaa and Nasr-El-Din (2011) showed that face plugging caused by in-situ polymer gelled acid occurred in low and high permeability core, and occurred more severely at lower flow rates.

Another approach, the use of viscoelastic (VES) acid systems, develops high viscosity by forming micellar structures to cross link the polymer chains. For this system to work, proper pH control is crucial for achieving the desired viscosity. At low pH values, the viscosity of the system is low, allowing the acid system to flow freely and penetrate deep into the subterranean matrix. On further increasing pH, the concentration of divalent calcium ions in solution increases during the reactions of acid with carbonates. The divalent ions begin associating with the micellar structures and eventually increase viscosity because of structure alternation. However, the viscosity of VES fluids can significantly reduce upon contacting with hydrocarbons. This may make it less favorable when used in treatment of dry-gas wells. The Surfactant–based VES acids were first introduced in the petroleum industry by separate groups, Chang et al. (2001). Also, some suggested that limited penetration of acid into the formation due to

relatively fast reaction rates can cause unfavorable consumption of the injected acid near the wellbore preventing development of deep penetrating wormholes and, even worse, decreasing the formation integrity in the near wellbore regions due to face dissolution. Addition of emulsified acids were extensively used in matrix stimulation. HCl is usually used as the internal phase of the emulsion and diesel is used as external oily phase, acting as a diffusion barrier to promote the creation of deep wormholes. However, successful application of matrix-acid treatments in heterogeneous formations or large-permeability-contrast formations appears necessary by requiring a diverting-agent stage and then treatment of the well with the emulsified acid. Hill and Jones (2003) showed that the stability of the emulsion is significantly reduced as the concentration of corrosion inhibitor increases, particularly under elevated temperature conditions.

3.3 Advantages of Nanoparticle-Based In-Situ Gelled System

Based on the results of nano dispersion and formation damage tests , fumed metal oxide nanoparticles are selected as the gelling agent for an in-situ gelled acid to divert the acidic fluid from high permeability zones into low permeability zones and achieve deep penetration of wormholes into the rock samples tested. In our nanoparticle-assisted acid formulation, magnesium chloride is introduced to modify the surface properties of the silica nanoparticles to achieve “instant” gelation under proper pH conditions.

It is believed that the key designing step to creating strong gels is that the associated hydroxyl groups on the nano silica surfaces react with the added cations, especially magnesium and water molecules in aqueous solutions. The coupling reactions lead to

generation of densely charged surfaces; the magnitude and sign of these surface charges strongly depend on solution pH and the amount of magnesium ions present.

To avoid early abandonment of producing wells due to naturally or man-made formation damage, an acidizing treatment is commonly implemented to effectively dissolve acid-soluble contaminants. One of the key criteria to a successful acidizing treatment is diversion. Developing additional suitable nanoparticle-based in-situ gelled acid formulations and the emulsified acid systems can drastically retard uncontrolled dissolution of rock surfaces and offer a range of solutions to achieve deeper penetration of the acid treatment under a wide range of subterranean conditions. For example, we plan to modify the current formulation and develop a series of optimal formulations which can provide the best performance for improving production under various subterranean situations and different crude oil properties. These treatments could also have the advantages of both in-situ gelled acid and emulsified acid systems and can be combined into a single novel stimulation fluid. Especially, in-situ gelled acid can be used in other conformance control purposes such as reservoir management and environmental impact mitigation to drastically reduce unwanted water production and enhance recovery performance without significant injectivity losses. We expect that this new acidizing formulation will have great potential on helping operators reducing lifting costs and environmental concerns as well as maintaining the longevity of the producing wells. The process could quickly impact oil shale production in Northeast Oklahoma by providing an effective water cutoff treatment for wells that produce excessive amounts of unwanted formation water that are currently disposed of in salt-water injection wells, which have been connected to induced seismicity.

4. Propagation of Nanofluid into Indiana Limestone Cores

4.1 Rheology Study of Nanofluid

Twenty five mL samples were prepared with 70:30 ratio of silica (Aerosil 200) to alumina (Aeroxide AluC) and a total nanoparticle concentration of 2.5 vol % with 97.5 vol% deionized water. The samples were mixed with vortex and used a horn sonicator with 25% amplitude for 20 minutes. After that pH of the samples were adjusted by diluted 2% HCl and NaOH stock solutions.

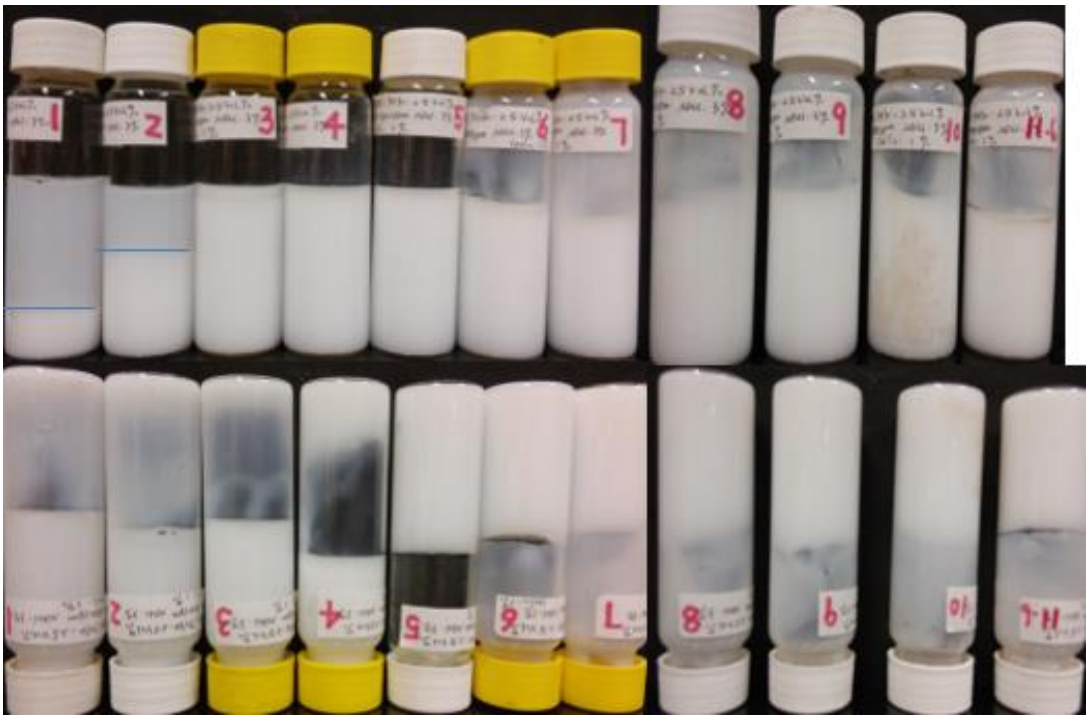


Fig 4-1. 2.5 vol% silica/alumina gelation at different pH

The pH of the sample was then adjusted using 10% NaOH and HCl solutions. Independent samples were prepared for each pH value tested to avoid dilution in the

nanoparticle gel via addition of further NaOH or HCl solution. The gelation region is between pH 5 to 11.6 as shown in Fig 4-1.

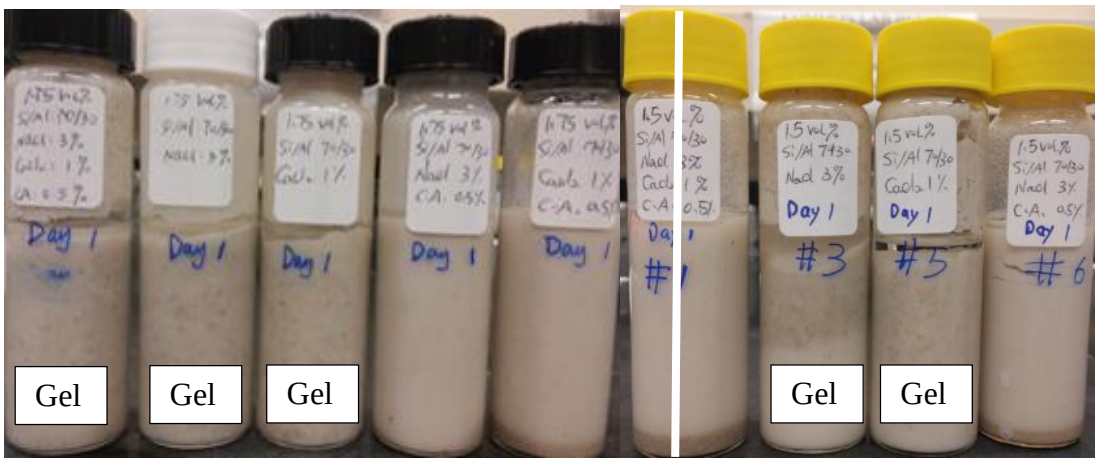


Fig 4-2. 1.75 vol%(left) 1.5 vol%(right) silica/alumina gelation with crushed Indiana limestone

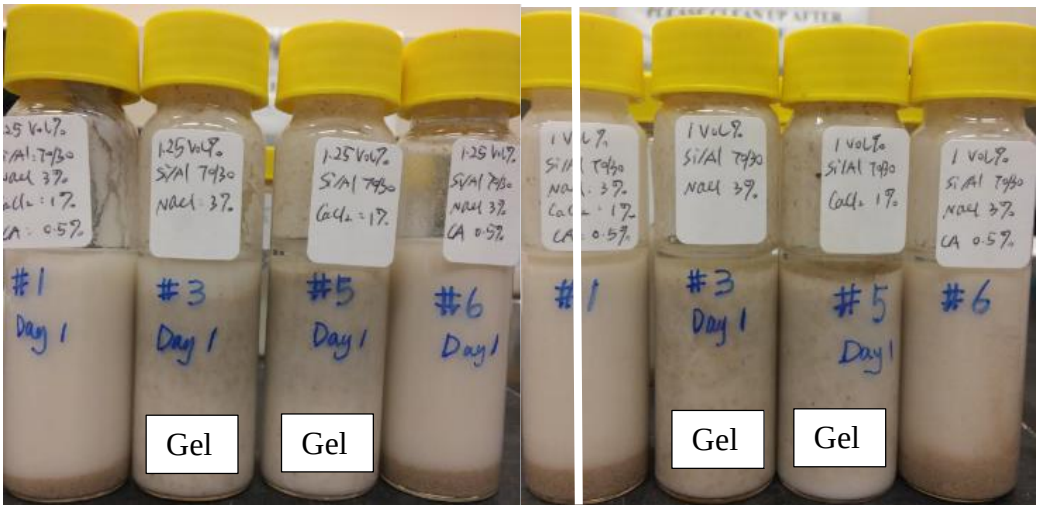


Fig 4-3. 1.25 vol%(left) 1 vol%(right) silica/alumina gelation with crushed Indiana limestone

Figs. 4-2 and 4-3 show that the gelation can be formed relatively lower vol% of total nanoparticles by adding crushed Indiana limestone. The volume fraction of nanoparticles needed to create gelation is actually decreased from 2.5 vol% to 1vol% by mixing 5g of crushed Indiana limestone. 75% deduction in total vol% of nanoparticles was achieved to create gelation which can also reduce permeability alteration and injection pressure during coreflood experiments. Adding the crushed Indiana limestone clearly enhance the gelation due to its strong affinity to water molecules. We hypothesized that some of the minerals fall off from the Indiana limestone after a reaction between hydrochloric acid and the rock surface, may promote gelation so that lower volume fraction is needed to create gel.

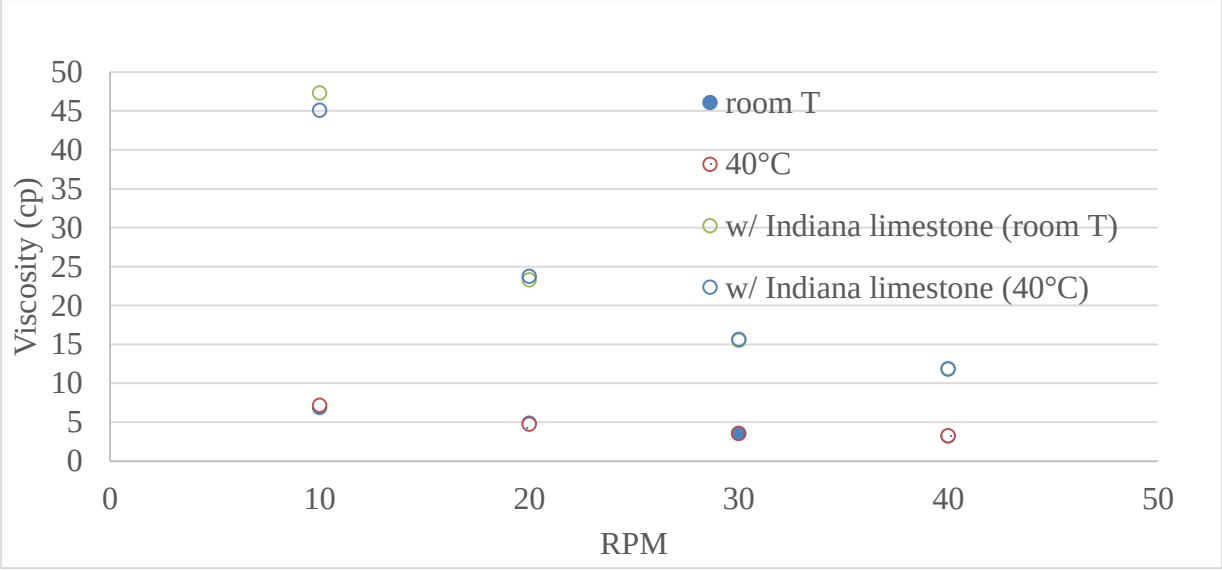


Fig 4-4. Viscosity comparison 0.75 vol%(right) silica/alumina gelation with crushed Indiana limestone

The group of 0.75 vol% silica/alumina samples were used to analyze difference in viscosity with and without crushed Indiana limestone. Fig 4-4 shows, a significant increase in viscosity when crushed Indiana limestone was added for both room temperature and 40°C and it is a shear thinning fluid. The fundamental concept of our acid-nanoparticle system is to create in-situ gelled acid when the mixture of silica and alumina form pseudo-solid shear thinning gels. The desired gel is formed by strong interparticle interactions at specific pH values, particle concentrations, shear rate, and temperature.

4.2 Coreflood Experiments for Acidizing

Mineral oil was used to displace nanofluid and Indiana limestone cores (1.5 inch in diameter, 6 inches long) were used. Fig 4-5 shows setups for coreflood experiment. Cores have two different permeability ranges (2~4md, 70~80md) in order to observe the propagation of gel and pressure profile. The nanofluid contains silica/alumina mixtures in 15 wt% hydrochloric acid and 3 wt% NaCl. The objective of the coreflood experiments was to evaluate how nanoparticle propagate when fluid containing high volume fraction (0.75~1 vol%) with 15% HCl is injected. Since lower fraction (0.01~ 0.5 vol%) of nanoparticles were not able to propagate through 8~10md cores in previous permeability impairment tests, our hypothesis was that if the nanoparticles are injected with hydrochloric acid, the nanoparticles are transported into a high flow channel which is the new wormhole created by hydrochloric acid.



Fig 4-5. Coreflood apparatus

Test A, B, C were performed with 2~4 md cores and Test D, E, F performed with 70~80 md cores with 1100 psi back pressure. Tables 4.1 and 4.2 summarized the operational conditions of each set of tests, low and high permeability cores, respectively.

System	Test A : 15% HCl	Test B : 1 vol% Si/Al 70/30, 3% NaCl, 15% HCl	Test C : 1 vol% Si/Al 70/30, 3% NaCl, 15% HCl
Porosity	15%	20 %(a used core with a wormhole pre-existed)	15%
Permeability	2~4md	2~4md	2~4md
Temperature	90°C	90°C	90°C
Max Upstream	1600 psi / 230 psi	1200 psi /	1800 psi / 1200 psi

Pressure/dp		**less than 30 psi**	
Flow rate	**3.5 ml/min**	**3.5 ml/min**	**3.5 ml/min**

Table 4-1. Test conditions for low permeability coreflood experiments

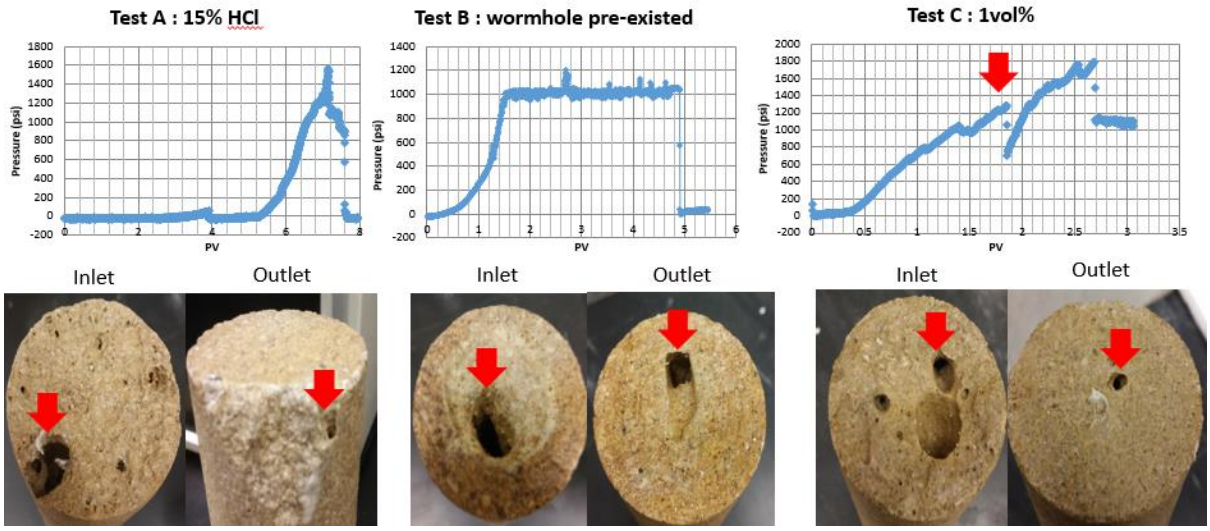


Fig 4-6. Pressure profiles and images of core faces (low perm)

In Test A, a 15 wt% hydrochloric acid-only was injected as the baseline case. The maximum injection pressure was around 1600 psi and the pressure difference, dp, across the core was around 450 psi. The volume fractions of nanoparticles used in Test B and C were determined based on the gelation tests implemented with crushed Indiana limestone. The core sample for Test B has a pre-existed wormhole generated in a separate test to prove that the nanoparticles can propagate through the core when a high flow channel present from the inlet to the outlet of the core. Maximum pressure was 1200 psi and the nanoparticles were successfully propagated through the core with less than 30 psi of dp.

The propagation of nanoparticle was confirmed by visual observation of the effluent samples. After the nanofluid injection was completed in Test B, the original wormhole size enlarges from 1mm to 8~9mm. In Test C, more face dissolution was observed at the inlet of the core compared to the baseline case of Test A and it shows 200 psi higher injection pressure and cyclic pressure behavior due to the in-situ gel created by nanofluid. The propagation of nanoparticles with creating a wormhole by acid reaction was confirmed with these coreflood experiments.

System	Test D : 15% HCl	Test E : 0.75 vol% Si/Al 70/30, 3% NaCl, 15% HCl	Test F : 1 vol% Si/Al 70/30, 3% NaCl, 15% HCl
Porosity	15%	16%	15%
Permeability	70~80md	70~80md	70~80md
Temperature	90°C	90°C	90°C
Max Upstream Pressure/dp	1100 psi / 120 psi	1150 psi / 95 psi	2300 psi / 1100 psi
Flow rate	3.5 ml/min	3.5 ml/min	3.5 ml/min

Table 4-2. Test conditions for high permeability coreflood experiments

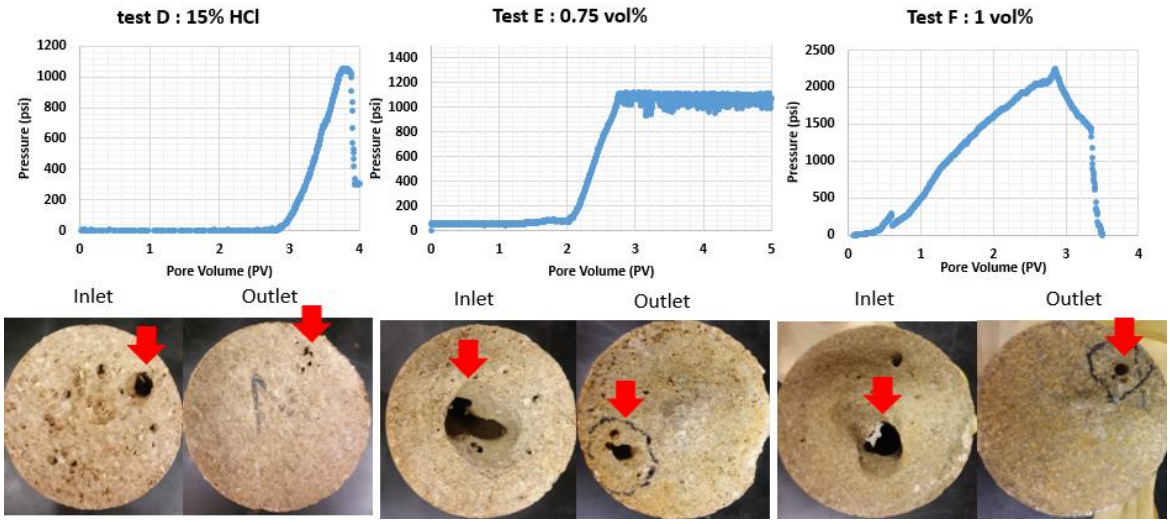


Fig 4-7. Pressure profiles and images of core faces (high perm)

Different volume fractions of nanoparticles applied in Test E and F were chosen based on the rheology tests implemented with crushed Indiana limestone because 0.75 vol% of silica/alumina with 3% NaCl did not form gel, instead 1 vol% of silica/alumina with 3% NaCl formed capable to form strong gel.

Similarly, in test Test D, a baseline of 15 wt% hydrochloric acid was injected to show a typical acid treatment. The maximum injection pressure was around 1100 psi and maximum dp across the core was around 120 psi. 70md core has much lower injection pressure and dp than 2~4md coreflood tests since nanofluid can flow more efficiently through the porous media having less time to breakthrough at higher permeability cores, so that the acid reaction occurs in a shorter period. Tests E and F were performed to confirm that there is a transition of gelation region from 0.75 vol% to 1 vol% based on the previous phase behavior tests with crushed Indiana limestone. As depicted in Fig 4-

7, the injection pressure profile shows that there is much more pressure resistance from Test F than that of Tests D and E due to the presence of the in-situ gels generated. There are also more face dissolutions on the inlet of the core for both Tests E and F. Note that adjustment of reaction rate or mass transport rate is needed to avoid face dissolution and optimize wormhole formation. The structure of the wormhole channels depends on the kinetics of the surface reaction between the acid/rock and the rates of mass transfer which varies from different fluid/mineral systems (Fredd 1999). Previously, the Damkohler number was used and closely related with these transport and reaction processes, and typically a single master curve could be plotted with the normalized number of pore volume to breakthrough versus the inverse of the Damkohler number (Fredd 1999). Since acid-nanoparticles system increases fluid viscosity and reduces the rate of acid transfer to the rock surface, the extent of transport/reaction should be more intensively studied to refine the optimum kinetic parameters for better prediction of the most efficient wormhole formation under various conditions. Another important consideration for controlling the wormhole length is the rate of fluid losses from the wormholes to heterogeneous formation matrix (Williams 1979). For instance, when natural fractures are present in the formation, the fractures dominate on acid leakoff over micro-fractures and matrix and the acid leakoff can be controlled by mechanisms of viscous flow (Mou 2011).

4.3 Slug Size Design

The design of a matrix acid treatment for a carbonate formation related to acid type and volume, the maximum injection rate and pressure below fracture pressure (Williams 1979). Fracture gradient from prior fracturing treatments can be expressed as shown in equation (3).

$$g_f \cong \alpha + (overburden\ gradient - \alpha)\frac{reservoir\ pressure}{depth} \quad (3)$$

Where, α is a constant (0.33 to 0.5) and the overburden gradient is about 1 psi/ft at depth less than 10,000 ft and 1 to 1.2 psi/ft at depths greater than 10,000 ft. Then the maximum possible injection rate without fracturing is obtained in equation (4).

$$i_{max} = \frac{4.917\times10^{-6}k_{av}h_n(g_f\times depth - reservoir\ pressure)}{\mu \ln(\frac{r_e}{r_w})} \quad (4)$$

Where,k_{av} is the average formation permeability with respect to the effect of the damage zone. Permeability is expressed in md, pressure in psi, viscosity in cp, and thickness in ft giving i_{max} in bbl/min.The injection rate to avoid fracturing must clearly be lower than i_{max}

The maximum surface pressure can be predicted as shown in equation (5).

$$p_{max} = \left(g_f - acid\ hydrostatic\ gradient\right)depth \quad (5)$$

Lastly, the volume and type of acid is determined. However, it is a rough estimation due to uncertainties in near wellbore conditions and geological variations. In general, an

emulsified acid is good for high permeability or naturally fractured reservoirs and a larger volume of acid is needed in deep and high temperature reservoirs injecting from 50 to 200 gal of 15%~28% per foot of interval perforated (Williams 1979).

There are several field examples with polymer based in-situ gelled acids. Field data in seawater injectors indicated that the acid system can cause loss of well injectivity when large volumes of in-situ gelled acid was used (Mohamed 1999). The volume of in-situ gelled acid should not exceed 30 vol% of the total volume of acids which is equivalent to 0.5 PV injection of ion-situ gelled acid. A viscoelastic acid was used in highly heterogeneous carbonate reservoirs (Cohen 2010). They concluded that pressure increase observed during the injection of a diverter should not be always considered as a direct indication of diversion and permeability contrast and total kh should be considered for the proper evaluation of treatments.

4.4 Conclusions

- Binary Silica / Alumina nanofluid has a shear thinning behavior and critical gelation concentration is decreased as crushed Indiana limestone added.
- Silica / Alumina nanofluid can be propagated into 70~80 md Indiana limestone cores.
- Relatively higher differential pressure was observed during nanofluid injection compared to 15% HCl coreflood test due to the viscosity increase in nanofluid.

5. Surface Modification of Silica Nanoparticles

5.1 Introduction

Understanding the acid-base behavior of silica surfaces is important for the modification of silica nanoparticles. One of the most common interfacial chemical reactions is the deprotonation of silanol (SiOH) groups at water-silica interfaces (Brinker 1990). Deprotonation creates negative surface charges and in particular, structural details of deprotonated SiOH groups determine the binding of ions and molecules to immersed silica surfaces and the overall surface charge density (Leung 2010). In this chapter, different types of monovalent and divalent cations were used to modify the silica surfaces and in particularly, magnesium ion has been identified as an ideal crosslinking agent effectively adsorbed onto the surface of silica creating sticky spots for gel network.

For designing purpose, gelation tables were first created at different temperatures and salts to study the effects of different ions altering the silica surface properties. The optimum system was chosen by the lowest critical gelation concentration and the fastest

gelation rate. The system was further investigated with different pH conditions and the viscosity was compared.

5.2 Gelation Tables (Effects of concentration and temperature)

Silica nanoparticles were mixed with different type salts such as $MgCl_2$, $CaCl_2$, NaCl, and KCl. The concentration silica nanoparticles and salts were varied and studied at two temperatures: room temperature and 90°C. These gelation tables illustrate how the gelation region different from the concentration of silica with respect to the concentration of different salts at different temperatures.

	Si 0.5 vol%	Si 0.75 vol	Si 1 vol%	Si 1.25 vol%
MgCl2 1%	X	X	X	X
MgCl2 3%	X	X	X	X
MgCl2 5%	X	X	X	O
MgCl2 7%	X	O	O	O
MgCl2 9%	X	O	O	O

<MgCl2>

	Si 0.5 vol%	Si 0.75 vol	Si 1 vol%	Si 1.25 vol%
CaCl2 1%	Δ	Δ	Δ	Δ
CaCl2 3%	Δ	Δ	Δ	Δ
CaCl2 5%	Δ	Δ	Δ	Δ
CaCl2 7%	Δ	Δ	Δ	Δ
CaCl2 9%	Δ	Δ	Δ	Δ

<CaCl2>

	Si 0.5 vol%	Si 0.75 vol%	Si 1 vol%	Si 1.25 vol%
NaCl 4%	X	X	Δ	Δ
NaCl 8%	X	X	Δ	Δ
NaCl 12%	X	X	Δ	Δ
NaCl 16%	X	Δ	Δ	Δ
NaCl 20%	X	Δ	Δ	Δ
NaCl 24%	X	Δ	Δ	Δ

<NaCl>

	Si 0.5 vol%	Si 0.75 vol%	Si 1 vol%	Si 1.25 vol%
KCl 4%	X	X	X	Δ
KCl 8%	X	Δ	X	Δ
KCl 12%	X	Δ	Δ	Δ
KCl 16%	X	Δ	Δ	Δ
KCl 20%	X	Δ	Δ	Δ
KCl 24%	X	X	Δ	Δ

<KCl>

Table 5-1 Gelation Table for room temperature, X: no gel, O : gel, Δ : gel after 24hr

In the tables, the symbol X stands for no gel, Δ stands for gel formed after 24 hours, and O means an instant gel. For example, 0.75 vol% Si and 7% $MgCl_2$ is needed to form an instant gel at room temperature as shown in Table 5.1. Higher concentration of Si and $MgCl_2$ helps to form an instant gel. Magnesium ions can effectively bridge between particles, creating large network-like structure. After 24 hours of retention time period, $CaCl_2$, KCl, and NaCl cases can also form gelation and $CaCl_2$ is more effective to form gelation due to higher charge density in Calcium ions than Potassium and Sodium. However, higher concentration of Si and salts can facilitate to form gel in overall.

	Si 0.5 vol%	Si 0.75 vol%	Si 1 vol%	Si 1.25 vol%
MgCl2 1%	Δ	Δ	Δ	Δ
MgCl2 3%	Δ	Δ	Δ	Δ
MgCl2 5%	Δ	Δ	Δ	O
MgCl2 7%	Δ	O	O	O
MgCl2 9%	Δ	O	O	O

<MgCl2>

	Si 0.5 vol%	Si 0.75 vol%	Si 1 vol%	Si 1.25 vol%
CaCl2 1%	Δ	Δ	Δ	Δ
CaCl2 3%	Δ	Δ	Δ	Δ
CaCl2 5%	Δ	Δ	Δ	Δ
CaCl2 7%	Δ	Δ	Δ	Δ
CaCl2 9%	Δ	Δ	Δ	Δ

<CaCl2>

	Si 0.5 vol%	Si 0.75 vol%	Si 1 vol%	Si 1.25 vol%
NaCl 4%	Δ	Δ	Δ	Δ
NaCl 8%	Δ	Δ	Δ	Δ
NaCl 12%	Δ	Δ	Δ	Δ
NaCl 16%	Δ	Δ	Δ	Δ
NaCl 20%	Δ	Δ	Δ	Δ
NaCl 24%	Δ	Δ	Δ	Δ

<NaCl>

	Si 0.5 vol%	Si 0.75 vol%	Si 1 vol%	Si 1.25 vol%
KCl 4%	Δ	Δ	Δ	Δ
KCl 8%	Δ	Δ	Δ	Δ
KCl 12%	Δ	Δ	Δ	Δ
KCl 16%	Δ	Δ	Δ	Δ
KCl 20%	Δ	Δ	Δ	Δ
KCl 24%	X	Δ	Δ	Δ

<KCl>

Table 5-2 Gelation Table for 90°C, X: no gel, O: gel, Δ : gel after 5~7hr

In Table 5.2, 0.75 vol% Si and 7% $MgCl_2$ formulation still forms an instant gel at 90°C and all of the other formulations creates gelation after 5 to 7 hours. These data reveal that increase of temperature dominates phase behavior over the concentrations of silica nanoparticles and salts. However, the trend with higher concentration of Si and $MgCl_2$ preferably forming an instant gel still remains true. Elevated temperature may work better to form gelation due to the destruction of natural hydrogen bonded network of water which is favorable for both mono- and di-valent cations to be adsorbed on the silica surface and help to build gel networks.

5.3 pH Sensitivity

The acidities of surface silanol groups are assigned to different chemical connectivities or inter-silanol hydrogen bonding (Leung 2010). It is the "temporary structure" of the agglomerates and can be accounted by the breaking of hydrogen bridge linkages. As pH increases, more silanol groups are deprotonated and silica surfaces become more negatively charged. Since these negatively charged surfaces can react with cations and facilitate gelation.

In Table 5.3, 1.25 vol% Si + 9% $MgCl_2$ forms gelation between pH 3 and pH 11. This indicates that addition of $MgCl_2$ offers superior gelation performances than equal amounts of 9% NaCl and 9% $CaCl_2$ due to higher charge density resulted in more deprotonated silanol groups on the surfaces at higher pH. Soft gel with 1.25 vol% Si +

9% $MgCl_2$ formulation was also formed even at low pH 3. However, hard gel was formed between pH 4 and pH 11 as shown. Soft gel was defined as the gelation with influence by gravity. In other words, soft gel will fall when the test vial is flipped upside down whereas hard gel has no impact by the gravity. Usually, hard gel stays on the bottom of the test vial for weeks when it is flipped upside down.

pH	9% NaCl	9% MgCl2	9% CaCl2
1	X	X	X
2	X	X	X
3	X	soft gel	X
4	X	Gel	X
5	X	Gel	X
6	X	Gel	X
7	X	Gel	X
8	X	Gel	X
9	X	Gel	X
10	soft gel	Gel	soft gel
11	soft gel	Gel	soft gel

Table 5-3 pH sensitivity of 1.25 vol% Si in different salts

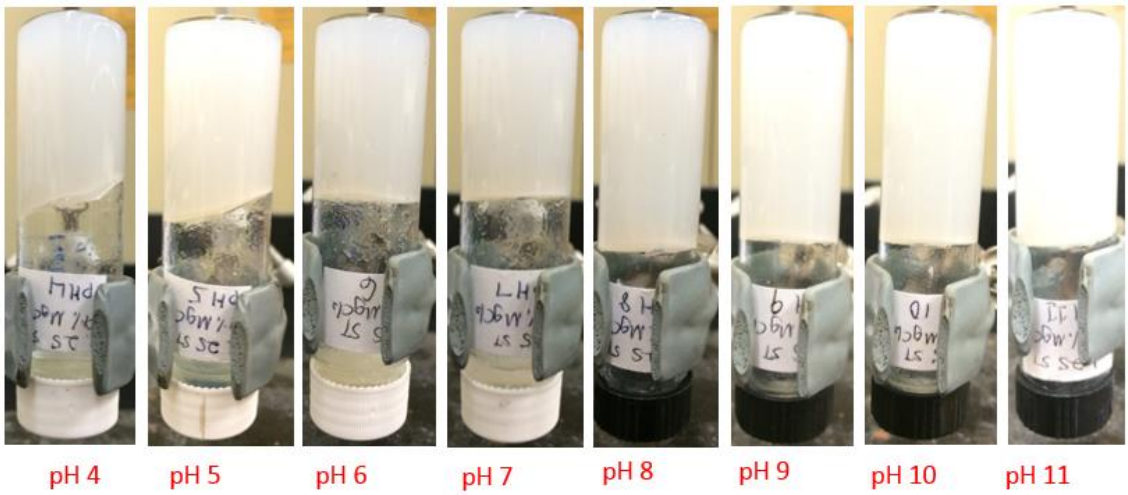


Fig 5-1 1.25 vol% Si+ 9% $MgCl_2$ at different pH

5.4 Zeta Potential and Mean Aggregate Size

Zeta potential data supports the previous pH sensitivity analysis on gelation region. In Fig 5-2, overall trend is that zeta potential becomes more negative along increase of pH due to the deprotonation of SiO2 surface. However, silica with salts added show that zeta potential is significant less negative or closer to zero at higher pH. In other words, salts compress the diffuse layer of the particles and become less stable. This instability introduces more aggregation of silica nanoparticles and 1.25 vol% Si + 9% $MgCl_2$ shows the absolute values of zeta potential get smaller (<10 mv) in the gelation region between pH 3 and pH 9. Also, mean aggregate size was measured by ZetaPals (Brookheaven) as shown in Fig 5-3. The results clearly indicate that the mean aggregate size is much bigger in the gelation region with the surface modification by $MgCl_2$.

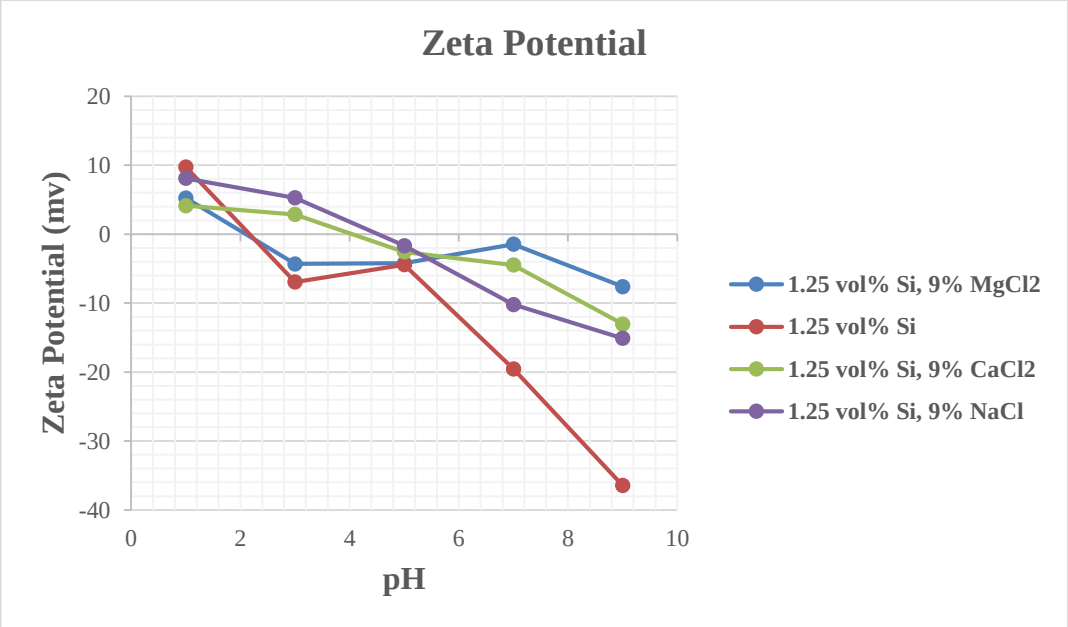


Fig 5-2 Zeta potential of silica at different pH

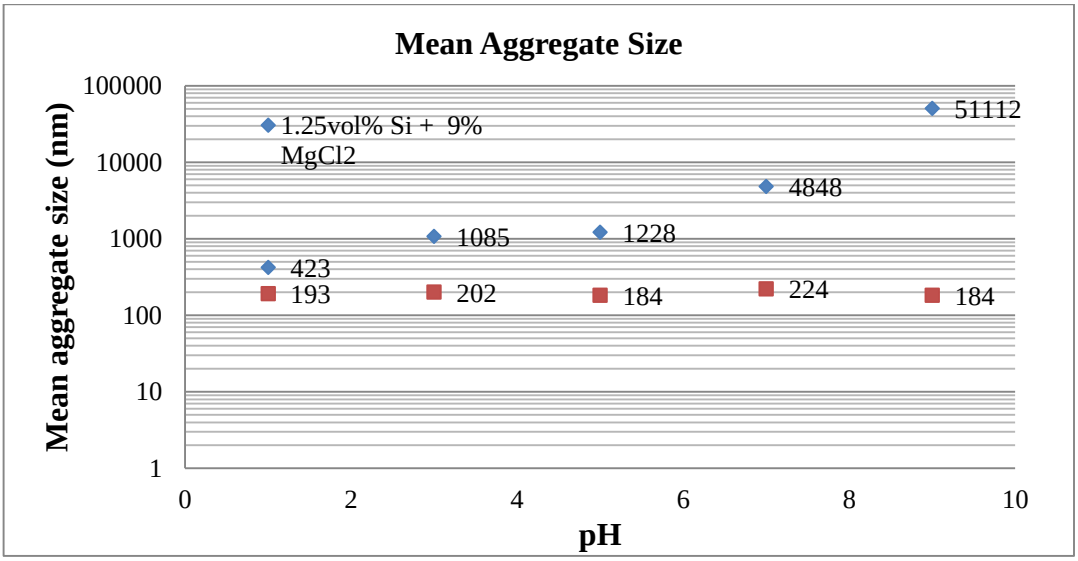


Fig 5-3 Effect of MgCl2 on mean aggregate size

5.5 Rheology Studies (Effects of shear rates, concentration of Si and salts)

The process of gelation is still not well understood. The formation of such oxide gels occurs through hydrolysis and polycondensation which are extremely complex having a rate constant depending drastically on the pH, composition, and temperature of sol-gel of alcoholic alumatrane solutions (Ksapabutr 2003). The rheology of silica gel prepared from mixtures of silicon oxide-$MgCl_2$-water varying shear rates, concentration of silicon oxide and $MgCl_2$ was studied under basic neutral conditions at 25°C during the gelation process. The gelation shows non-Newtonian pseudoplastic behavior from the time of preparation near the gelation point.

A torsional rheometer (SR5000 Rheometric Scientific) is used to measure the steady-shear and complex viscosity of nanofluid at low shear rates and Fann viscometer is used for high shear rates due to its instability during the tests in the torsional rheometer with small sample size. Fann viscometer is known as the Standard of the Industry for drilling fluid viscosity measurements. The test sample is contained in an annular space or shear gap between the cylinders and Fann produces a range of true Couette coaxial cylinder rotational viscometers as shown in Fig 5-5. Through precision gearing, it operates the rotation of the outer cylinder with known velocities and the viscous drag exerted by the fluid creates a torque on the inner cylinder or bob. This torque is transmitted to a precision spring and its deflection is measured.



Fig 5-4 Torsional Rheometer

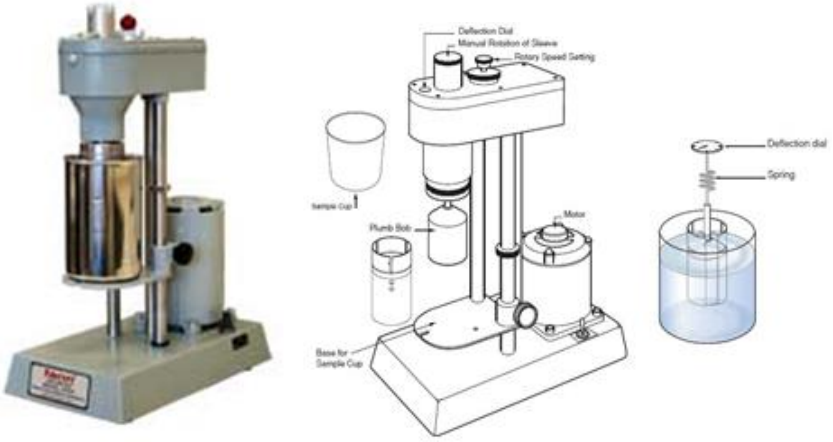


Fig 5-5 Fann viscometer

The viscosity of silica gel was compared at 0.75/1/1.25 vol% Si + 0/3/5/7/9 wt% $MgCl_2$ at different shear rates. Fig 5-6 clearly exhibit different degrees of shear thinning behaviors between all samples tested. However, 1.25 vol% Si + 9% $MgCl_2$ sample shows the most drastic decrease in viscosity as shear rate increases. Data listed in Table 5.4 loosely defines different viscosity regimes such as viscous, soft gel, hard gel, and no gel. No gel region is defined with viscosity less than 10 cp. Viscous region is defined with viscosity between 10^2cp and 10^3cp. Soft gel region is defined with viscosity between 10^4cp and 10^9cp. Lastly, hard gel region is defined with viscosity between 10^{10}cp and 10^{13}cp.

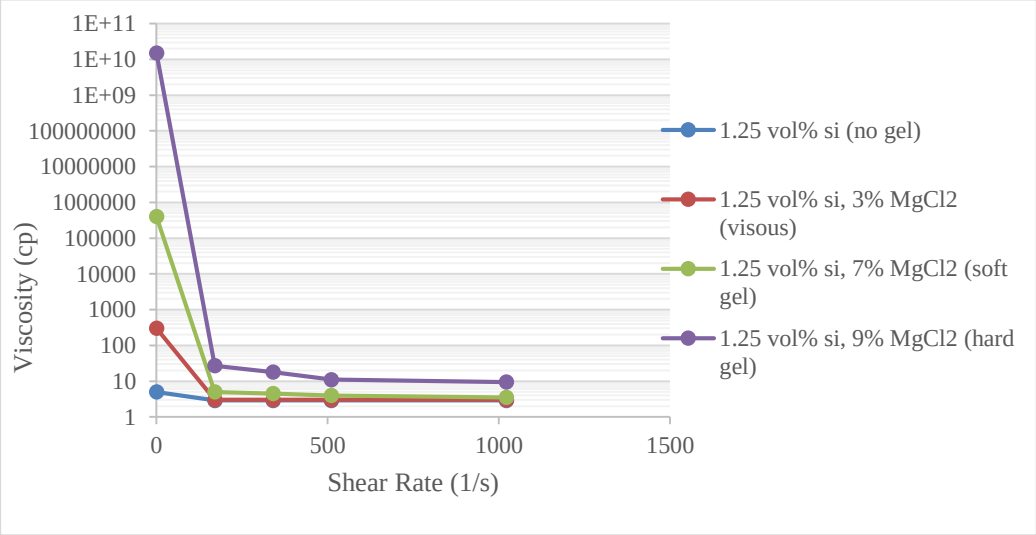


Fig 5-6 Viscosity comparison with different concentration of $MgCl_2$

	Si 0.5 vol%	Si 0.75 vol%	Si 1 vol%	Si 1.25 vol%
MgCl2 1%	X	X	X	X
MgCl2 3%	X	X	X	V
MgCl2 5%	X	V	V	S
MgCl2 7%	X	S	S	S
MgCl2 9%	X	O	O	O

<X: no gel (< 10cp), V: viscous ($10^{2\sim3}$cp) S: soft gel ($10^{4\sim9}$cp) O: hard gel ($10^{10\sim13}$cp)>

Table 5-4 Gelation table with Si + $MgCl_2$

In Fig 5-7, initial viscosity increases are observed 7% $MgCl_2$. For example, 0.75 vol% Si shows 3 cp up to 5% $MgCl_2$ and majority of data are overlapped (the colored symbols showed differently/unclearly in Fig. 5-7, maybe use different symbol shapes instead). However, 0.75 vol% Si + 7% $MgCl_2$ starts showing distinct deviations in viscosities which are two times greater than 0.75 vol% Si + 5% $MgCl_2$ sample. This similar trend is also observed in Figures 5-8 and 5.9 for high dosages of Si particles. The superior performance of $MgCl_2$ in terms of boosting viscosity is also confirmed in a comparison with $CaCl_2$, NaCl, and KCl in Fig 5-10. The viscosity is lower when $CaCl_2$, NaCl, and KCl are present in the solution compared with a sample with no salt added and there is no reasonable explanation found yet. Another general trend is that increase of silica concentration also effectively boosts the viscosity.

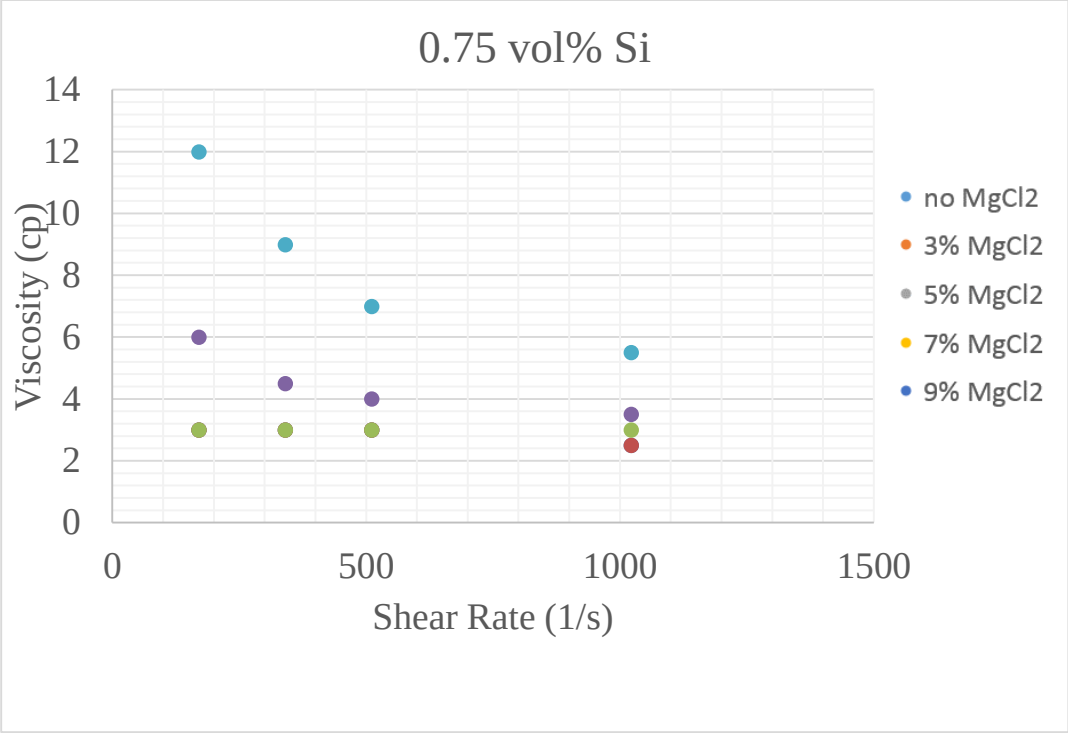


Fig 5-7 Viscosity of 0.75 vol% Si with different concentration of $MgCl_2$

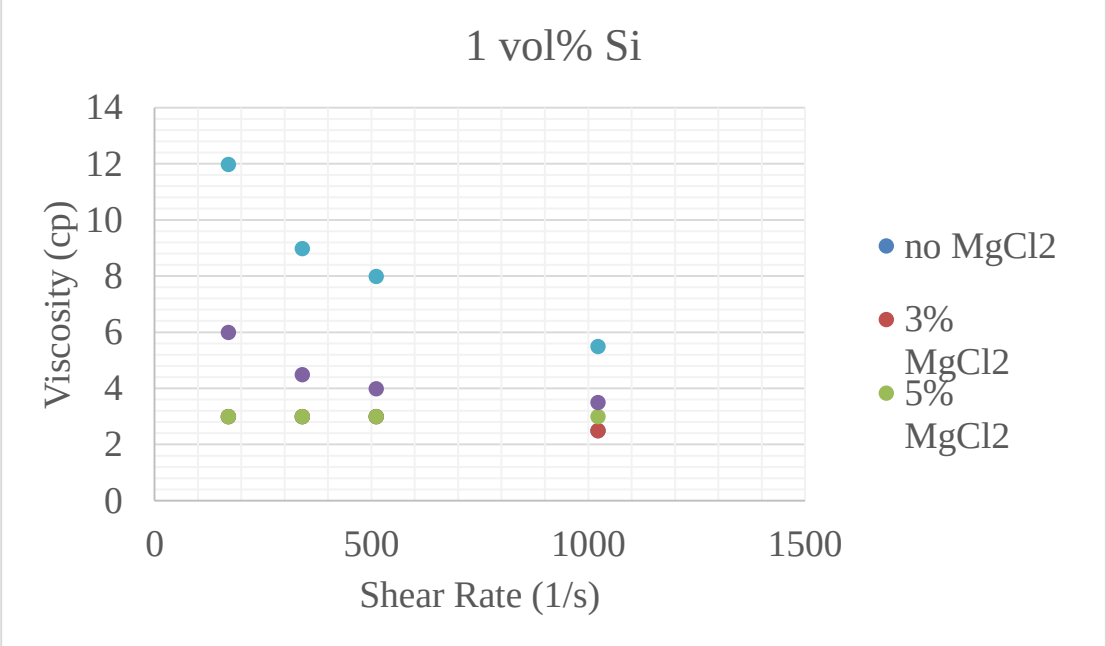


Fig 5-8 Viscosity of 1 vol% Si with different concentration of $MgCl_2$

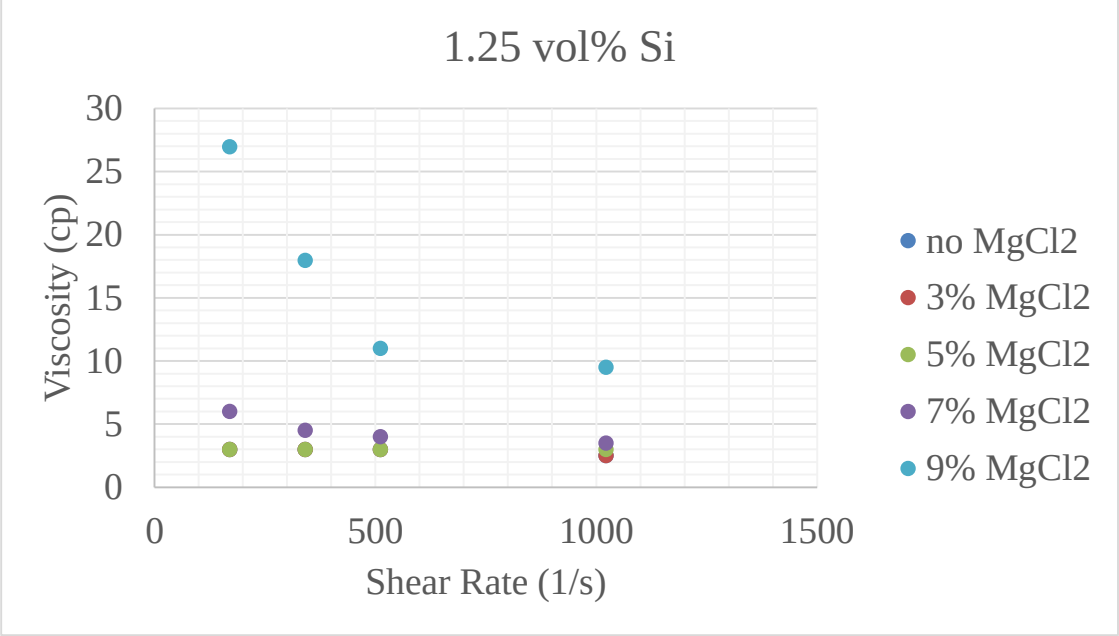


Fig 5-9 Viscosity of 1.25 vol% Si with different concentration of $MgCl_2$

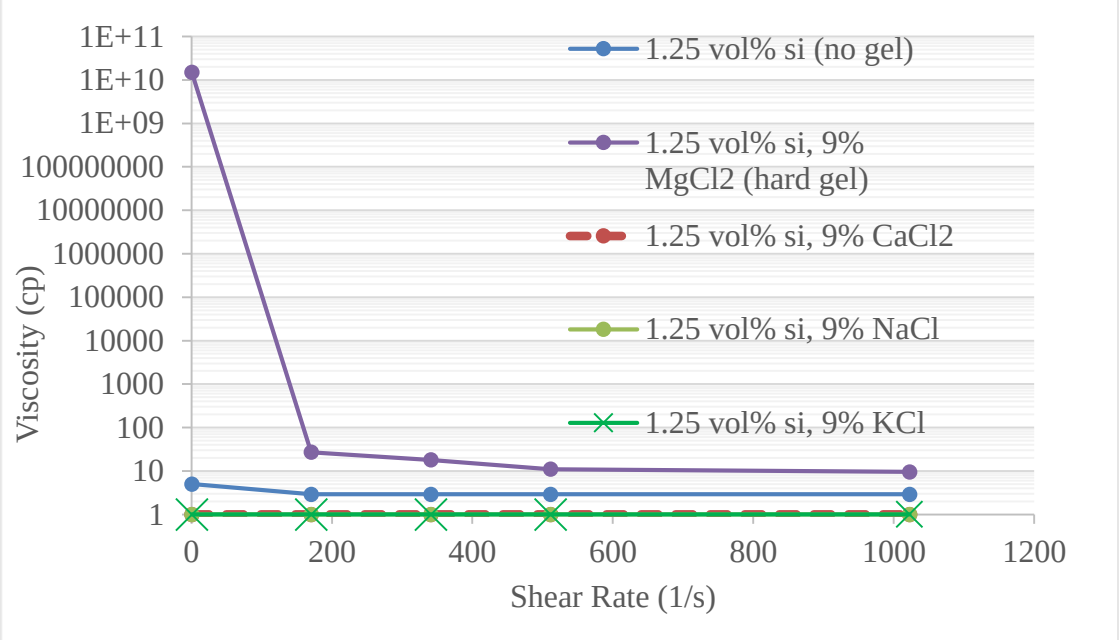


Fig 5-10 Viscosity of 1.25 vol% Si with different salts

5.6 Breaking Gelation

Once the nanofluid is injected into the targeted zone, gel is not wanted after the acid diversion. Thus, acid diversion is not only important, but also breaking gel is necessary in order to avoid permanent pore blocking or formation damage. There are three possible ways to easily break gelation. 1. Low pH (<pH 2) can break the gel by protonation on the surface silanol groups. Hydrogen bridging is no more effective at the low pH. 2. Applying shear rates into the gel, can break hard aggregates to soft aggregates. Some of the weakly bonded network can be broken apart and the viscosity dramatically decreases. 3. Reducing the concentration of silica can decrease the viscosity. The dilution of silica can minimize the amount of hard aggregates and make the system below critical gelation concentration. These three methods are very effective and laboratory experiments were performed as one example of lowering solution pH shown in Fig 5-11.

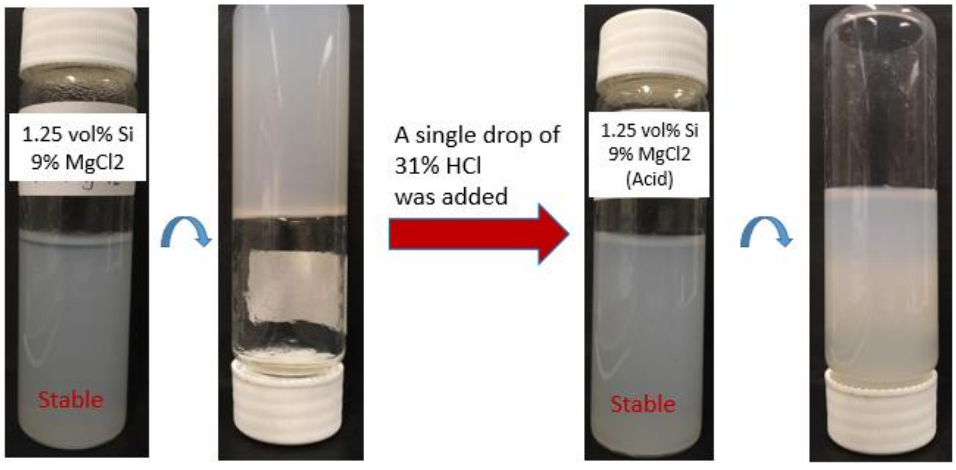


Fig 5-11 Breaking gelation

In a second example test, Fig 5-12 shows the presence of gelation in the wormhole of Indiana limestone core and it is put into a core holder and water was injected with 1 ml/min at 90 °C. The core was selected with a pre-existing wormhole and fully immersed in the nanofluid (1.25 vol% Si + 9% $MgCl_2$) for 24 hours in order to make gelation in the wormhole. Instant gel breaking was confirmed after injecting fresh water with water breakthrough in a few minutes and differential pressure less than 1 psi.



Fig 5-12 Gelation in the core

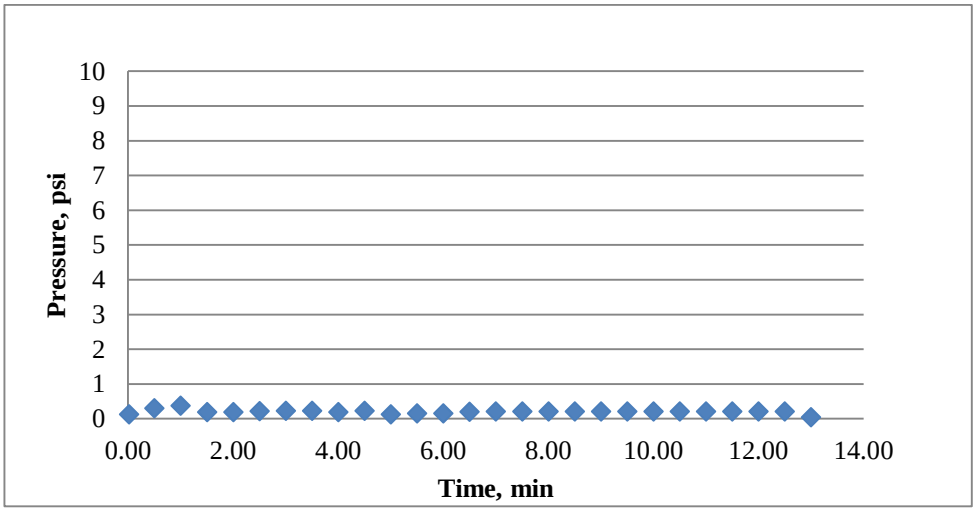


Fig 5-13 Differential pressure through Indiana limestone core during gel breaking test

5.7 Conclusions

- Addition of 7% $MgCl_2$ can effectively form an instant gel with 0.75 vol% Si and increase of temperature can drastically minimize gelation time.
- There is an optimum pH region for gelation due to its change in surface property by protonation at low pH and deprotonation at high pH.
- Zeta Potential shows that $MgCl_2$ can modify overall surface charge on silica.
- Mean aggregate size significantly increases with increasing in pH since there are more negatively charged silanol group sites to react with Mg^{2+} ions.
- Rheology data indicate that it is a shear thinning fluid. Thus, viscosity can be easily controlled by shear rates.
- Shear force, dilution of silica nanoparticles, and low pH (<pH 2) can break gelation.

6. A Study of Diversion Using Nanoparticle-Based In-Situ Gelled Acids System

6.1 Sandpack Test

One dimensional column tests were used in this study to simulate one-dimensional flow through crushed Indiana limestone. Valuable information obtained from the column study include: gelation enhancement under flow-through conditions, potential plugging in the formation by the gelation. The procedures for setting up a column are briefly described below. Indiana limestone was gently crushed and sieved through sieving trays to get a specific grain size. Permeability of 3 inch long and 1 inch in diameter sandpack was measured base on the stable differential pressure of the samdpack column once it reaches steady state during flow tests with various flow rates. A total of 9% $MgCl_2$ was used to pre/post flush the column and different injection strategies such as flow rates, concentrations of silica or the presence of $MgCl_2$ were investigated to optimize the system to form gelation into the column. Before the injection of nanofluid, pH of nanofluid was adjusted by citric acid which is a weak acid to make solution pH lower than 4. Thus, high viscous gel is not initially formed before the nanofluid injection. After the acid reaction between nanofluid + citric acid and Indiana limestone, pH increases due to the production of water from the reaction. This increase in pH induces nanofluid to move into gelation region.

Fig 6-1 shows the design of the single and parallel sandpack tests. In parallel sandpack tests, two different permeability sandpacks were prepared and nanofluid was co-injected into both columns to investigate flow pattern in the columns simultaneously. Isco pump

was used in constant flow mode throughout the tests. Two separate accumulators were used for $MgCl_2$ and nanofluid. The recovery of silica nanoparticles were confirmed by UV-vis.

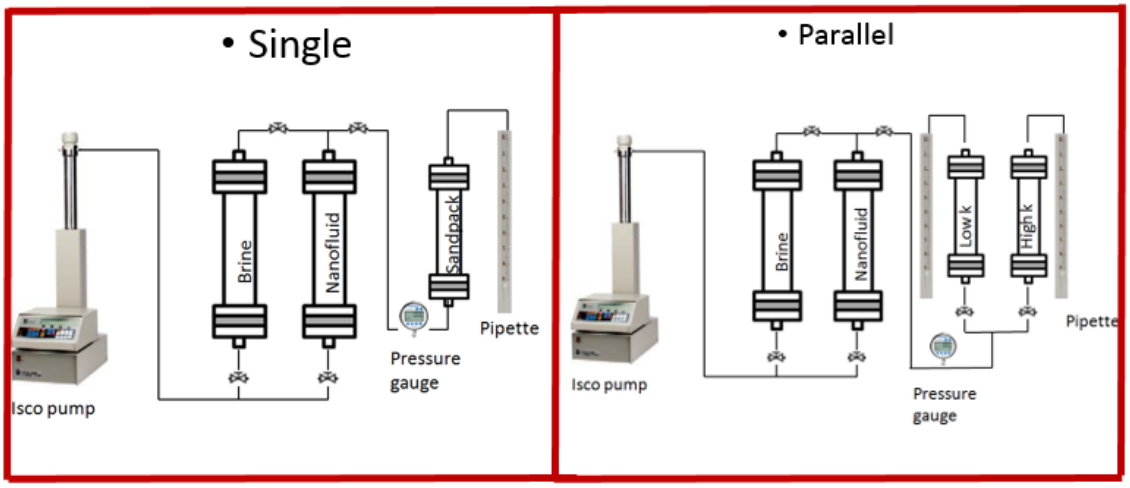


Fig 6-1 Sandpack test design



Fig 6-2 Sandpack test apparatus

Table 6-1 shows the properties of porous media like porosity and permeability as well as test conditions such as flow rates, temperature, and different types of nanofluid. From test 1 to test 4, flow rate, temperature, permeability, and porosity were fixed and only nanofluid injection strategy was different. For example, one pore volume of 1.25 vol% Si + 9% $MgCl_2$ and three pore volume of 0.5 vol% Si + 9% $MgCl_2$ plugged sandpack in test 2 and test 4. However, nanofluid without $MgCl_2$ did not plug the sandpack. This indicates that the presence of $MgCl_2$ is crucial to form gelation into the porous media and it is an effective cross linker to build gel network.

	Test 1	Test 2	Test 3	Test 4
Permeability	200~300md	200~300md	200~300md	200~300md
Porosity	32%	32%	32%	32%
Flow rate	1 mL/min	1 mL/min	1 mL/min	1 mL/min
Temperature	RT	RT	RT	RT
Pre/Post-flush	MgCl2	MgCl2	MgCl2	MgCl2
Nano-injection (with CA 0.05 %)	1PV of 1.25 vol% Si	1PV of 1.25 vol% Si +MgCl2	3PV of 0.5 vol% Si	3PV of 0.5 vol% Si +MgCl2
Total Si recovery	96%	N/A, Plugged	> 100%	N/A, Plugged
Max. Injection Pressure	2 psi	>25 psi	<1psi	>25 psi

Table 6-1 Sandpack tests with different nanofluid formulations

In Table 6.2, three different shear rates were tested since our nanofluid is shear thinning fluid. The change in shear rates can introduce different range of viscosity. The hypothesis was that Test 5 applying lower flow rate induced gelation more effectively due to the higher viscosity and eventually plugged the sandpack. These tests provide some initial confidences for parallel coreflood tests since enough viscosity increase is needed for in-situ gelled acid to plug or slow down the flow instantly in the higher permeability core so that the following acid can injected into the lower permeability core.

	Test 5	Test 6	Test 7
Permeability	5 Darcy	5 Darcy	5 Darcy
Porosity	34%	34%	34%
Flow rate	0.1 mL/min	0.5 mL/min	1 mL/min
Temperature	RT	RT	RT
Pre/Post-flush	9% MgCl2	9% MgCl2	9% MgCl2
Nano-injection (with CA 0.05 %)	1PV of 1.25 vol% Si +9% MgCl2	1PV of 1.25 vol% Si +9% MgCl2	1PV of 1.25 vol% Si +9% MgCl2
Max. Injection Pressure	>25 psi (plugged)	16.4 psi	10 psi

Table 6-2 Sandpack tests with different flow rates (shear rates)

In Figs 6-3 to 6-5, the conductivity measurements show the change in hydrodynamic before and after nanofluid injection. Since there is plugging in test 5, no conductivity measurements are available. However, it is clear that the formation was plugged and hydrodynamic changed completely because postflush with $MgCl_2$ was unable to perform due to plugging. Figs 6-4 and 5 show that there is no change in hydrodynamic before and after the nanofluid injection since conductivity values for pre and post flush with deionized water were not change much.

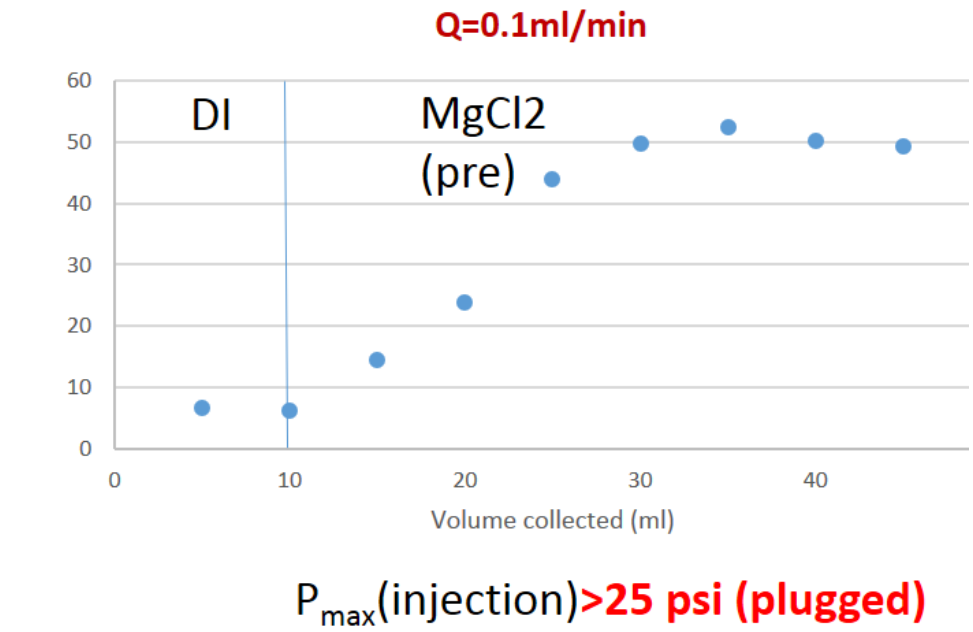


Fig 6-3 Conductivity measurements during Test 5

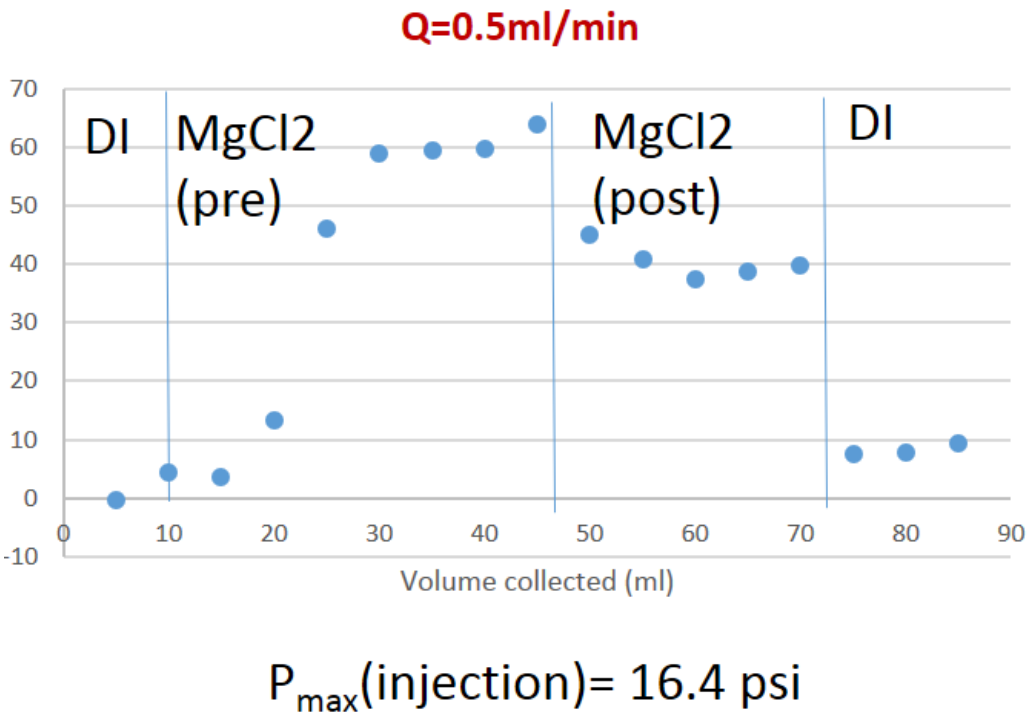


Fig 6-4 Conductivity measurements during Test 6

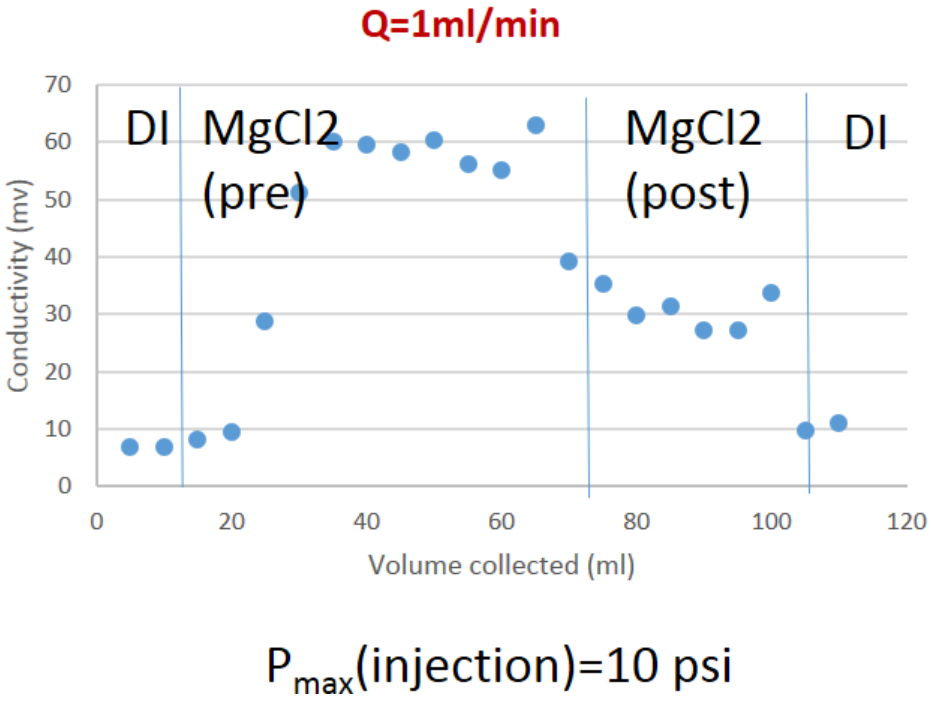


Fig 6-5 Conductivity measurements during Test 7

Parallel sandpack tests are used to give a credibility for parallel coreflood tests to divert acid into the lower permeability core. Thus, plugging in the high permeability sandpack is desired to confirm the in-situ gel mechanism. Two sandpacks installed with 3 inch long and 1 inch in diameter core plugs were prepared and the selected nanofluid was co-injected into both sandpacks simultaneously. Again, 9% $MgCl_2$ brine was used during pre- and post-flush of the column and also contained in the injected nanofluid. The nanofluid pH was adjusted by citric acid which is a weak acid to maintain solution pH

below 4. During parallel sandpack tests, low permeability is 200 md and high permeability is about 3 Darcy.

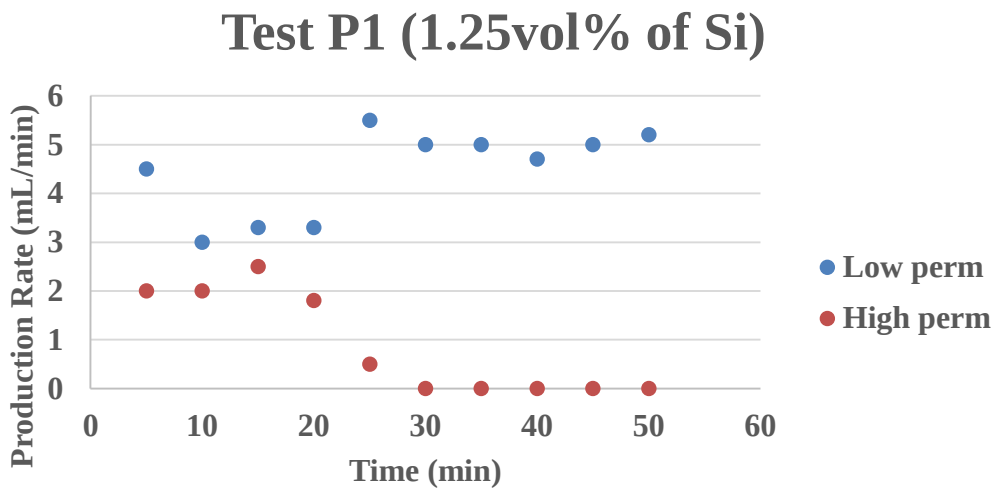


Fig 6-6 Production rate comparison between high and low perm sandpacks during Test P1

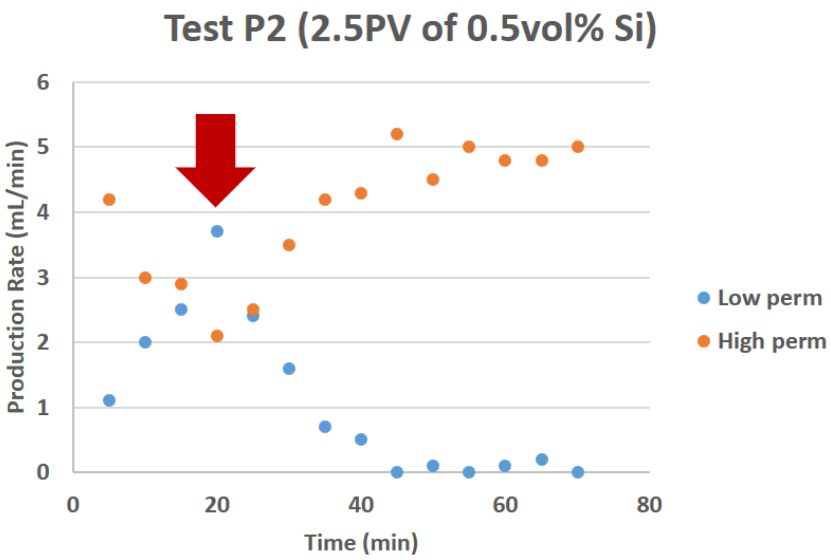


Fig 6-7 Production rate comparison between high and low perm sandpacks during Test P2

Nanofluid used in P1 test is one pore volume of 1.25 vol% Si + 9% $MgCl_2$ and 2.5 pore volume of 0.5 vol% Si + 9% $MgCl_2$ was used for P2 test. P1 test shows plugging after 30 mins in Fig 6-6 and there is a flip of production rate on P2 test at 20 mins in Fig 6-7.

This indicates that 1.25 vol% Si + 9% $MgCl_2$ system almost instantly slow down the flow in the high perm column and completely plugged the formation after 30 mins. However, after 2.5 pore volumes injection of low level formulation, 0.5 vol% Si + 9% $MgCl_2$, was unable to completely plug the high perm column. The flip of production rate on P2 test after 20 min injection can be related to a filtration effect on small pore throats but injection rate was high enough to apply enough shear forces to break big hard aggregates.

6.2 Coreflood Experiments for Diversion

This section discusses a new single stage stimulation fluid that is both self-diverting and deep penetrating in carbonate reservoirs. Surface modified silica form yield stress gels at a specific pH range, which helps to reduce injectivity into high permeability zone so that the acid can flow into the low permeability zone. The gel is an effective fluid-loss additive that optimizes acid dissolution of the carbamate to be more uniform and produce multiple deep penetrating wormholes. Single and parallel coreflood tests were implemented to study the flow of nanoparticle-based acids in porous media. The cores used in the experiments have the permeability range of 2 to 70 md.

Injection of surface modified silica effectively forms instant gels at volume fractions as low as 0.75% at neutral pH due to electrostatic heteroaggregation into networks. Higher

concentration of silica and magnesium chloride exhibit stronger gel strength at room temperature and form gelation faster at a higher temperature.

The single coreflood results indicate that the nanoparticle-based acids create multiple wormhole paths for both low (2 md) and high (70 md) permeability cores and the acid is diverted into a low permeability core during parallel coreflood experiments. This stimulation fluid can divert the acid and generate multiple wormholes simultaneously in both low and high permeability cores.

System Indiana Limestone	Test S1 : 15% HCl Low k	Test S2 : 15% HCl High k	Test S3 : 1.25 vol% Si + 15% HCl + 9% $MgCl_2$ Low k	Test S4 : 1.25 vol% Si + 15% HCl + 9% $MgCl_2$ High k	Test S5 : 1.25 vol% Si + 15% HCl + 9% $MgCl_2$ Low k	Test S6 : 1.25 vol% Si + 15% HCl + 9% $MgCl_2$ High k	Test S7 : 1.25 vol% Si + 15% HCl + 9% $MgCl_2$ Field Core
Porosity	15%	15%	15%	15%	15%	15%	13%
Permeability	2 md	70 md	2md	70 md	2md	70 md	< 10md
Temperature	90°C	90°C	90°C	90°C	Room Temperature	Room Temperature	90°C
Max Pump Pressure	700 psi	400 psi	1600 psi	2100 psi	1260 psi	1020 psi	2200 psi (Pback=1100 psi)
Flow rate	3.5 ml/min	3.5 ml/min	3.5 ml/min	3.5 ml/min	3.5 ml/min	3.5 ml/min	3.5 ml/min
Acid Breakthrough	4.5 mins	8.3 mins	20 mins	12.8 mins	16.2 mins	12.5 mins	8 mins
Length	6 in	6 in	6 in	6 in	6 in	6 in	2.8 in

Table 6-3 Single coreflood tests

The main objective of single coreflood tests is to confirm the propagation of nanofluid into both low and high permeability cores as well as field core samples. The changes of key variables between these tests are permeability, temperature, and mineralogy of core. Table 6.3 shows that all tests have acid breakthrough which means both 15% HCl and nanofluid can be propagated into the cores. However, nanofluid tends to have slower acid breakthrough time since it is used as a retarded acid system creating in-situ gel. This also causes higher pressure environment during the run.

<Inlet of S1 and S2, 15% HCl HT>



<Outlet of S1 and S2, 15% HCl HT>

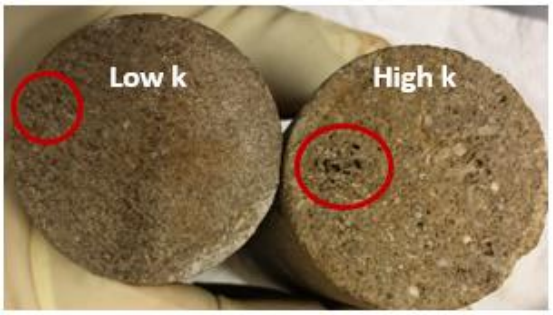


Fig 6-8 Core images for Test S1 and S2 with 15% HCl

<Inlet of S3 and S4, Nano HT>

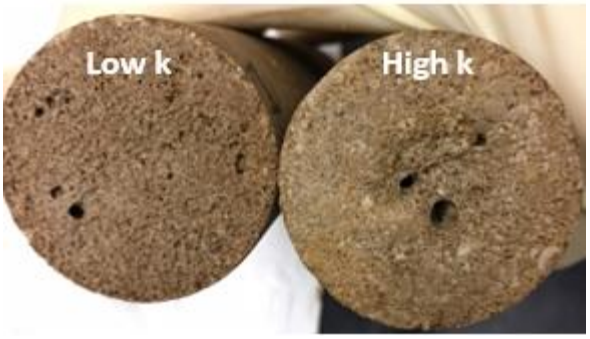


<Outlet of S3 and S4, Nano HT>



Fig 6-9 Core images for Test S3 and S4 with 1.25 vol% Si + 9% $MgCl_2$ + 15% HCl

<Inlet of S5 and S6, Nano RT>



<Outlet of S5 and S6, Nano RT>



Fig 6-10 Core images for Test S5 and S6 with 1.25 vol% Si + 9% $MgCl_2$ + 15% HCl

Figs 6-8 to 6-10 show that more numbers of wormhole were detected especially from the outlet of low perm cores in nanofluid injection and room temperature test has less face dissolution on the inlet surface. This concludes that test S5 is most successful run in terms of mild face dissolution and number of wormholes presented on the outlet of the core. However, parallel coreflood test is needed to confirm the effectiveness of diversion from high perm cores. These single coreflood tests indicate that nanofluid can be successfully propagated and it has tendency to have multiple wormholes due to its in-situ gel property.



Fig 6-11 Core inlet(left) and outlet(right) images for Test S7 with 1.25 vol% Si + 9% $MgCl_2$ + 15% HCl

Quartz	Calcite (CaCO3)	Chlorite (ClO_2^-)	Pyrite (FeS2)	Anhydrite (CaSO4)	Siderite (FeCO3)	Apatite ($Ca_5(PO_4)_3(F,Cl,OH)$)
0.99	70.366	10.654	10.551	2.559	4.375	0.505

Table 6-4 Mineralogy of Field Core

The field core used in Test S7 has different mineralogy compared to Indiana limestone. It has significant portion of pyrite (10.5%), siderite (4.4%), Calcite (70%) as shown in Table 6.4 and chlorite (10.6%) whereas Indiana limestone cores contain 99.8% of calcite and 0.2% of quartz. The different mineralogy can introduce different degree of reaction rate between acid and rock or dissolution rate of rock.

Parallel coreflood tests were implemented installed with two different permeability cores (2md vs. 70 md). The main objective of parallel coreflood tests is to confirm the diversion of acid into low permeability cores and create wormholes. The variables through tests are temperature, and type of injection fluid to compare the effectiveness of diversion. Flow rate, permeability, porosity is fixed. Fig 6-12 shows the parallel coreflood apparatus and Table 6.5 shows that only test P3 with 1.25 vol% Si + 9% MgCl2 + 15% HCl has a successful diversion at 90 °C.

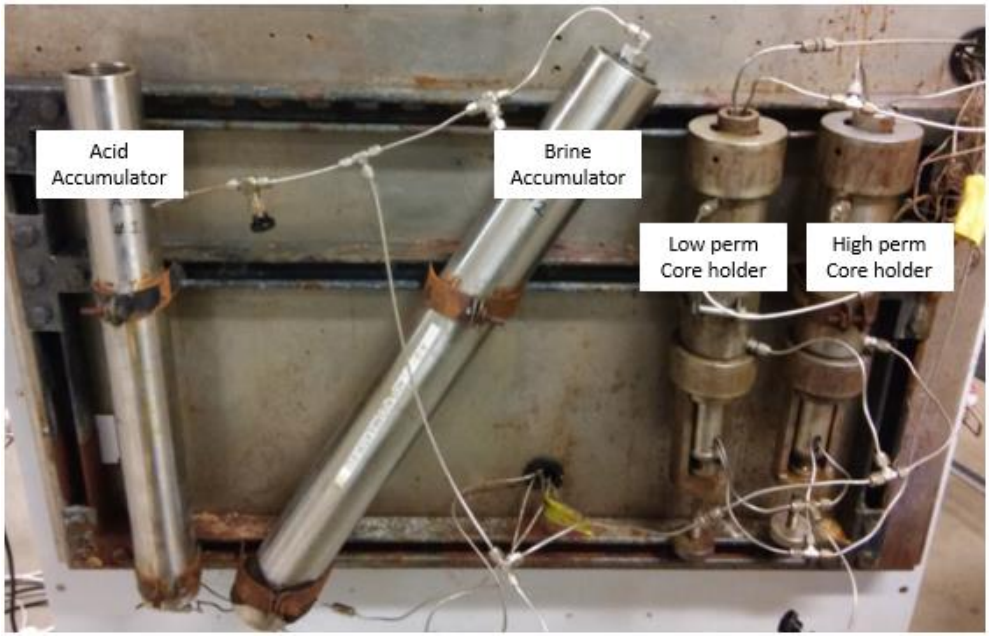


Fig 6-12 Parallel coreflood tests

System	Test P1 : 15% HCl Indiana Limestone	Test P2 : 1.25 vol% Si + 15% HCl + 9% $MgCl_2$ Indiana Limestone	Test P3 : 1.25 vol% Si + 15% HCl + 9% $MgCl_2$ Indiana Limestone
Porosity	15% for both cores	15% for both cores	15% for both cores
Permeability	2 md / 70 md	2 md / 70 md	2 md / 70 md
Temperature	90°C	Room Temperature	90°C
Max Pump Pressure	180 psi	450 psi	480 psi
Flow rate	3.5 ml/min	3.5 ml/min	3.5 ml/min
Acid Breakthrough time	High perm : 8 mins Low perm : N/A "No Diversion"	Test was aborted after 50 mins of injection. "No acid breakthrough"	High perm : 15 mins Low perm : 20 mins "Successful Diversion"

Table 6-5 Parallel coreflood tests

Only the higher perm core has a wormhole breakthrough in test P1 with 15% HCl as shown in Fig 6-13. This is because there is no in-situ gel to control conformance with viscosity boost. In Fig 6-14, mild face dissolution was observed on the surface of low perm core inlet in test P2 with nanofluid at room temperature. Acid reaction rate was not enough to create wormhole breakthrough on the outlet of both cores. Thus, there is no acid breakthrough both cores. Test P3 with nanofluid at 90°C has successfully divert the acid into low perm core. As shown in Fig 6-15, first breakthrough in high perm core was obtained in 15 mins and after 5 mins another wormhole breakthrough was found in low perm core.

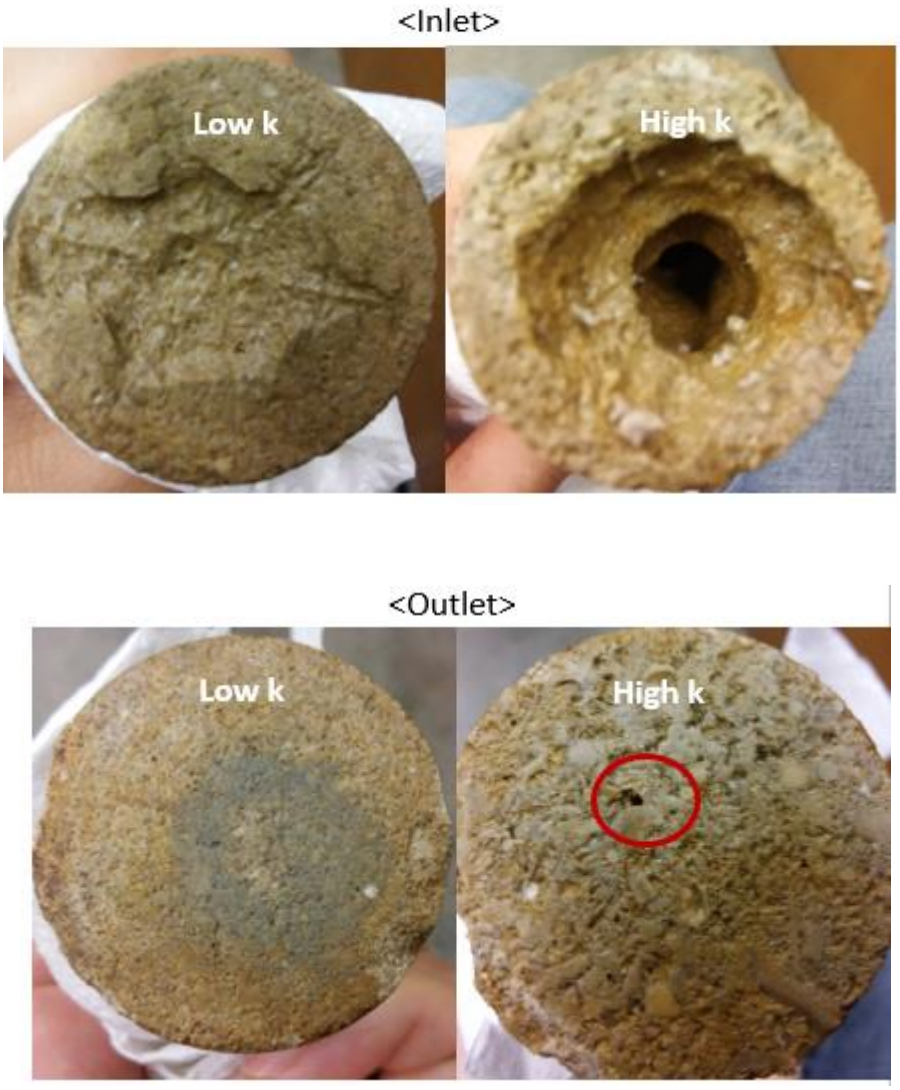
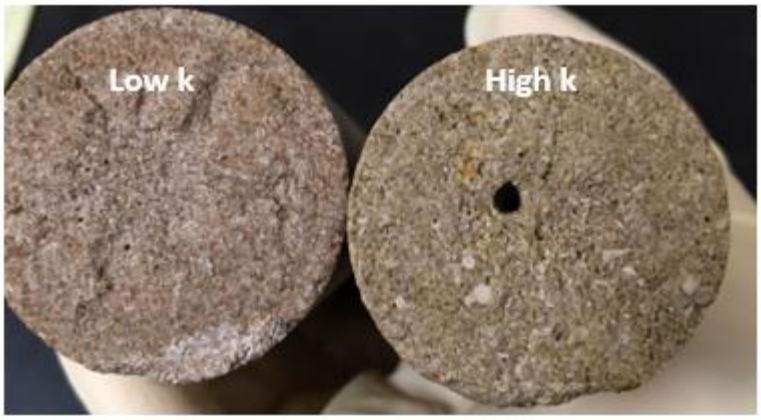


Fig 6-13 Core images for Test P1 with 15% HCl

<Inlet>



<Outlet>

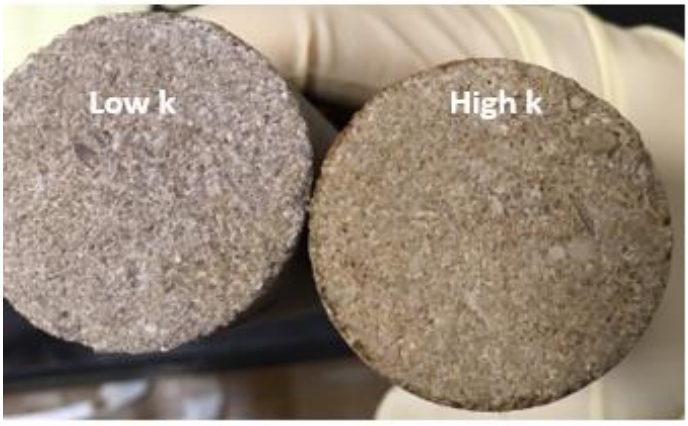
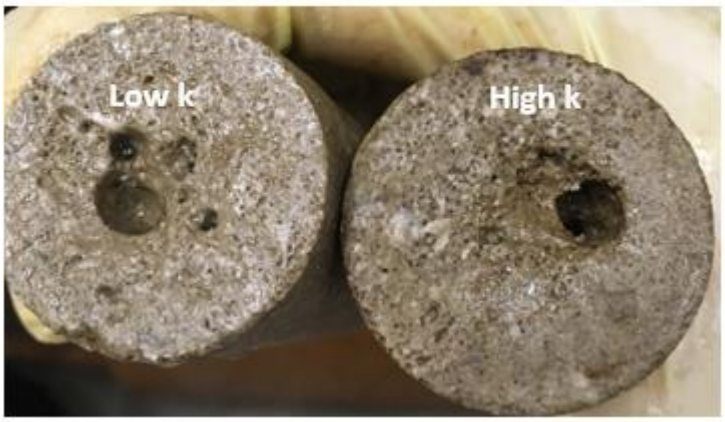


Fig 6-14 Core images for Test P2 with 1.25 vol% Si + 9% $MgCl_2$ + 15% HCl at room temperature

<Inlet>



<Outlet>

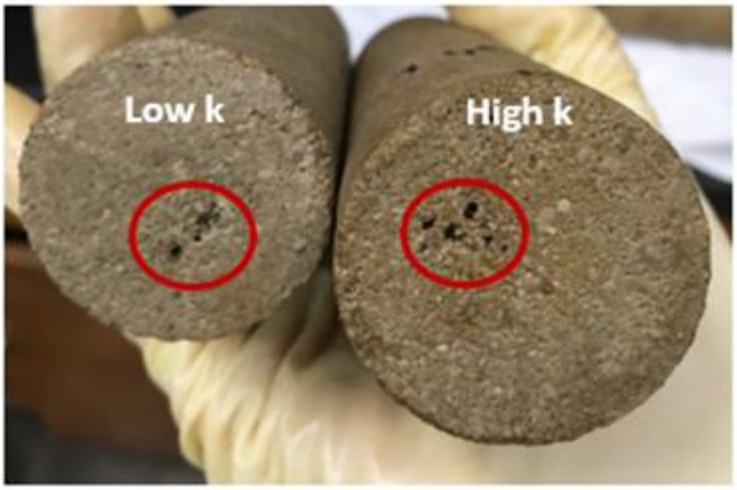


Fig 6-15 Core images for Test P3 with 1.25 vol% Si + 9% $MgCl_2$ + 15% HCl at 90° C

6.3 Effect of shear rate on the performance of nanoparticle-based in-situ gelled acid

From chapter 5, the viscosity behavior of the in-situ gelled acid is shear thinning and it is known that MgCl2 is an effective crosslinking agent to increase the viscosity. The dramatic change in viscosity was observed especially between 0.5 1/s and 200 1/s. Therefore, the further investigation on the actual shear rate in the core during the coreflood was implemented. The actual shear rate that the acid is subjected to the core can be calculated by (Rojas et al. 2008)

$$\gamma = \frac{u}{\emptyset L} \tag{3}$$

where u is the Darcy velocity, m/s ; ∅ is porosity, volume fraction; L is a characteristic length representative of the pore-scale velocity gradients, L=0.05; and D is the average pore-throat diameter. The pore size is estimated from permeability by taking the square root of the permeability in md (Dick et al 2000). The shear rates in each low and high permeability cores were 509.2 1/s and 84.8 1/s as shown in Table 6-6. This results show that the shear rate in high perm core is 10 $^{5\sim6}$ cp and the shear rate in low perm core is 10 cp. There is a dramatic contrast in viscosity of in-situ gelled acid in both cores which can help to divert the acid into the low perm core. During the parallel coreflood Test P3, after the first breakthrough from the high perm core, there was no effluent fluid coming out from the high per core outlet. However, there was a second acid breakthrough from the low perm core after 5 mins from the first breakthrough. This indicates that the actual shear rate in high perm core is within the viscosity range of soft gel (10^4cp ~ 10^9cp).

	low perm core	high perm core
Permeability (md)	2.0	70.0
Porosity (%)	15.0	15.5
Average pore throat diameter (um)	1.4	8.4
Flow rate (cm^3/min)	3.5	3.5
Darcy velocity (cm/s)	0.000972	0.000550
Shear rate (1/s)	509.2	84.9

Table 6-6 Calculated shear rates for low and high perm cores

6.4 Conclusions

- Sandpack test results confirm that 1.25 vol% Si + 9% $MgCl_2$ can form in-situ gel and plug both 200 md and 3 Darcy formation.
- Injection strategy such as concentration of silica and injection rate significantly influence the performance of in-situ gelation. The concentration of silica is directly related to critical gelation concentration and the injection rate controls shear force which is crucial to adjust viscosity for shear thinning fluid.
- From single coreflood tests, the results indicate that nanofluid can be successfully propagated and it has tendency to have multiple wormholes due to its in-situ gel property.
- Single stage nanofluid (1.25 vol% Si + 9% $MgCl_2$ + 15% HCl) can successfully divert the acid into low permeability core after the acid breakthrough from the high permeability core.

- At low shear rate in the high perm core, soft gel was formed inside of the core and it has the ability to change the direction of the acid into low perm core during parallel coreflood Test P3. A successful acid diversion was attained.

7. Conclusions and Recommendations

This study exhibits significant differences from other technologies and prior art in at least four aspects. 1. It results in a pseudo-solid gel which exhibits both strength and rigidity even at a very low volume fraction of nanoparticles. The fumed metal oxide particle's surface properties are successfully modified with addition of magnesium chloride and blending with concentrated hydrochloric acid. Once this treatment fluid directly contacts with carbonate rock, dissolution of the carbonate results in an increase of pH which leads to instantaneous generation of gel networks. The resulting gel exhibits pseudo-solid behavior when total particle volume fractions are kept greater than 0.75 %v/v in the presence of 7 wt% $MgCl_2$ at room temperature (23 °C). At elevated temperature (90 °C) the same formulation with 15% HCl added can produce instant soft gel networks which change to pseudo-solid gel after equilibrating for 35 minutes. 2. The instant gel system exhibits distinct shear thinning behavior. When no shear rate is applied, the solution forms a gel and the gel can be completely transformed into a low viscosity fluid by increasing the shear rate. In other words, the gel viscosity or the mechanical strength can be easily manipulated by altering the operating shear rate during acidizing treatment operations. Calculated shear rates during the coreflood tests shows that soft gel was initially formed in the high perm core since the viscosity

calculated in the high per core was in the range of soft gel. It is easy to control the viscosity of the fluid by calculating expected shear rates. Therefore, injection rate should be designed based on the expected shear rate in the formation. The newly developed formulation can be easily adjusted to apply for a variety of permeability contrast ratios between different depth of subterranean. 3.The new formulation possesses excellent tolerance of harsh salt and temperature conditions. In one example, a gel-producing, stable dispersion of nanoparticles was prepared with 20% of total dissolved solids (TDS) at 90°C. 4. This formulation is also a single-stage acidizing system that achieves the dual purposes of self-diversion and deep penetration, and so eliminates the need for multiple-stage operations via injection of different fluids sequentially. This can minimize the number of treatment stages and project cost in field applications. Currently, applying different fluid systems in multiple stages acidizing treatment drastically increases the logistical issues and complexity at the field and is much less favorable for the operation. Thus, this newly developed formulation provides significant improvements and benefits for acidizing treatment practice, both technically and economically.

Especially, in-situ gelled acid can be used in other conformance control purposes such as reservoir management and environmental impact mitigation to drastically reduce unwanted water production and enhance recovery performance without significant injectivity losses. We expect that the new acidizing formulation will have great potential on helping operators reducing lifting costs and environmental concerns as well as maintaining the longevity of the producing wells. The process could quickly impact oil shale production in Northeast Oklahoma by providing an effective water cutoff

treatment for wells that produce excessive amounts of unwanted formation water that are currently disposed of in salt-water injection wells, which have been connected to induced seismicity.

References

Al-Ibadi, Adnan, Faruk Civan. 2013. Evaluation of Near-Wellbore Formation Treatment by Gel Particles Using Dimensional Analysis. Presented at the SPE Production and Operations Symposium, Oklahoma City, Oklahoma, USA, 23-26 March. SPE-164507-MS. http://dx.doi.org/10.2118/164507-MS.

Alaskar, Mohammed N., Morgan F. Ames, Steve T. Connor et al. 2012. Nanoparticle and Microparticle Flow in Porous and Fractured Media--An Experimental Study. http://dx.doi.org/10.2118/146752-MS

Bobe R, Ferch H, Fratzscher H. 2006. Basic Characteristics of AEROSIL Fumed Silica. Technical Bulletin Fine Particles 11, Evonik Industries, Parsippany, NJ (July 2006)

Cerbelaud, M., A. Videcoq, P. Abelard et al. 2008. Heteroaggregation between Al2O3 submicrometer particles and SiO2 nanoparticles: Experiment and simulation (in English). *Langmuir* 24 (7): 3001-3008. <Go to ISI>://WOS:000254480500011.

Chang, Frank, Faruk Civan. 1991. Modeling of Formation Damage Due to Physical and Chemical Interactions Between Fluids and Reservoir Rocks. *Proc*. http://dx.doi.org/10.2118/22856-MS

Civan, Faruk. 2007. *Reservoir Formation Damage - Fundamentals, Modeling, Assessment, and Mitigation (2nd Edition)*, Elsevier (Reprint).

Clement C.F. Harrison R.G. 1992a. The coagulation of Radioactive Aerosols. Proc. European Aerosol Conference. Oxford. Sept. 1992. J. Aerosol Sci. 23. S145 - 148. http://dx.doi.org/10.1016/0021-8502(92)90370-B

Clement C.F. 1992b. The Charging of Radioactive Aerosols. Journal of Aerosol Science. Vol(23) : 481-504. http://dx.doi.org/10.1016/0021-8502(92)90019-R

Cohen C.E. Tardy P.M.J. Lesko Tim. Lecerf B. Pavlova S. Voropaev S. Mchaweh A. 2010. Understanding Diversion with Novel-Fiber-Laden Acid System for Matrix Acidizing of Carbonate Formations. *SPE Annual Technical Conference and Exhibition. Italy*. September 2010. http://dx.doi.org/10.2118/134495-MS

Dick, m.A., Heinz, T.J., Svoboda, C.F., and Aston, m. 2000. Optimizing the Selection of Bridging Particles for Reservoir Drilling Fluids. Paper SPE 58793 presented at the SPE International Symposium on Formation Damage, Lafayette, Louisiana. USA, 23-24 Febuary. http://dx.doi.org/10.2118/58793-MS

Fredd, C.N., Fogler, H.S., 1999. Optimum Conditions for Wormhole Formation in Carbonate. Porous Media: Influence of Transport and Reaction, *SPE Journal*, 4(3), 196-205. http://dx.doi.org/10.2118/56995-PA

Ghadimi, A., R. Saidur, H. S. C. Metselaar. 2011. A review of nanofluid stability properties and characterization in stationary conditions (in *International Journal of Heat and Mass Transfer* 54 (17–18): 4051-4068. http://www.sciencedirect.com/science/article/pii/S0017931011002304.

Gorrepati, E. A., P. Wongthahan, S. Raha et al. 2010. Silica Precipitation in Acidic Solutions: Mechanism, pH Effect, and Salt Effect (in English). *Langmuir* 26 (13): 10467-10474. <Go to ISI>://WOS:000279239900014.

Gruesbeck, C., R. E. Collins. 1982a. Entrainment and Deposition of Fine Particles in Porous Media. *SPE Journal*. http://dx.doi.org/10.2118/8430-PA

Gruesbeck, C., R. E. Collins. 1982b. Particle Transport Through Perforations. *SPE Journal*. http://dx.doi.org/10.2118/7006-PA

Hendraningrat, Luky, Li Shidong, Ole Torsaeter. 2012. A Glass Micromodel Experimental Study of Hydrophilic Nanoparticles Retention for EOR Project (Russian). *Proc*. http://dx.doi.org/10.2118/159161-MS

Hendraningrat, Luky, O. Torsæter. 2014. Understanding Fluid-Fluid and Fluid-Rock Interactions in the Presence of Hydrophilic Nanoparticles at Various Conditions. *Proc*. http://dx.doi.org/10.2118/171407-MS

Herzig, J. P., D. M. Leclerc, P. Le Goff. 1970. Flow of Suspensions through Porous Media-Application to Deep Filtration (in *Industrial & Engineering Chemistry* 62 (5): 8-35. http://dx.doi.org/10.1021/ie50725a003

Huang, Tianping, James B. Crews. 2008. Nanotechnology Applications in Viscoelastic Surfactant Stimulation Fluids. *SPE Production & Operations*. SPE-107728-PA. http://dx.doi.org/10.2118/107728-PA

Huang, Tianping, James B. Crews, Gaurav Agrawal. 2010. Nanoparticle Pseudocrosslinked Micellar Fluids: Optimal Solution for Fluid-Loss Control With Internal Breaking. Presented at the SPE International Symposium and Exhibiton on Formation Damage Control, Lafayette, Louisiana, USA, 10-12 February. SPE-128067-MS. http://dx.doi.org/10.2118/128067-MS

Huang, Tianping, James B. Crews, John Robert Willingham. 2008. Nanoparticles for Formation Fines Fixation and Improving Performance of Surfactant Structure

Fluids. Presented at the International Petroleum Technology Conference, Kuala Lumpur, Malaysia, 3-5 December. IPTC-12414-MS. http://dx.doi.org/10.2523/IPTC-12414-MS

Huang, Tianping, Brian Alan Evans, James B. Crews et al. 2010. Field Case Study on Formation Fines Control with Nanoparticles in Offshore Applications. Presented at the SPE Annual Technical Conference and Exhibition, Florence, Italy, 19-22 September. SPE-135088-MS. http://dx.doi.org/10.2118/135088-MS

Chang, Jing Song, S. Vigneswaran. 1990. Ionic strength in deep bed filtration (in *Water Research* 24 (11): 1425-1430.

Kalfayan, L.J., Production Enhancement with Acid Stimulation (2nd Ed.), 2008, PennWell

Karami, A. 2009. Study on modification of colloidal silica surface with magnesium ions (in English). *Journal of Colloid and Interface Science* 331 (2): 379-383. <Go to ISI>://WOS:000263335700018.

Ksapabutr, A. Bussarin., Gulari, B. Erdogan., Wongkasemjit, A. Sujitra., Sol-gel transition study and pyrolysis of alumina-based gels prepared from alumatrane precursor. Colliods and Surfaces A: Physicochem. Eng. Aspects 233. 2004 http://dx.doi.org/10.1.1.582.6876

Maheshwari. P., Maxey. J., Balakotaiah. V., Reactive-Dossolution Modeling and Experimental Comparison of Wormhole Formation in Carbonates with Gelled and Emulsified Acids. *SPE Production & operations*. 2015. http://dx.doi.org/10.2118/171731-PA

Mazzone, D. N., G. I. Tardos, R. Pfeffer. 1986. The Effect of Gravity on the Shape and Strength of a Liquid Bridge between 2 Spheres (in English). *Journal of Colloid and Interface Science* 113 (2): 544-556. <Go to ISI>://WOS:A1986E053700024.

McElfresh, Paul M., Marodi Wood, Daniel Ector. 2012. Stabilizing Nano Particle Dispersions in High Salinity, High Temperature Downhole Environments. *Proc*. http://dx.doi.org/10.2118/154758-MS

Mou, J., Zhang, S., Zhang, Y., Acid Leakoff Mechanism in Acid Fracturing of Naturally Fractured Carbonate Oil Reservoirs, *Transp Porous Med*., 2012, 91, 573-584

Mohamed, S.K., Nasr-El-Din, H.A., and Al-Furaidan, Y.A. 1999. Acid Stimulation of Mou, J., Zhang, S., Zhang, Y., Acid Leakoff Mechanism in Acid Fracturing of Naturally Fractured Carbonate Oil Reservoirs, *Transp Porous Med*., 2012, 91, 573-584.

Mora-Barrantes, A. Rodríguez , L. Ibarra , L. González and J.L. Valentín. 2011. Overcoming the disadvantages of fumed silica as filler in elastomer composites. Journal of Materials Chemistry (21): 7381-7392. http://dx.doi.org/10.1039/c1jm10410a

Mustin, Benjamin, Boris Stoeber. 2010. Deposition of particles from polydisperse suspensions in microfluidic systems (in English). *Microfluidics and Nanofluidics* 9 (4-5): 905-913. http://dx.doi.org/10.1007/s10404-010-0613-4

Navarrete. R. R., Holms. B.A, McConnell, .S.B. SPE European Petroleum Conference.1998. SPE-50612-MS. http://dx.doi.org/10.2118/50601-MS

Pittman Edward. 1992. Relationship of Porosity and Permeability to Various Parameters Derived from Mercury Injection-Capillary Pressure Curves for Sandstone. The American Association of Petroleum Geologists Vol (76) : 191-198.

Rabie, A.I., Gomaa, A.M., Nasr-El-Din, H.A., HCl/Formic In-Situ-Gelled Acids as Diverting Agents for Carbonate Acidizing, *SPE Production & Operations*, 2012, 5, 170-184. SPE 140138-PA. http://dx.doi.org/10.2118/140138-PA

Rodriguez Pin, Elena, Matthew Roberts, Haiyang Yu et al. 2009. Enhanced Migration of Surface-Treated Nanoparticles in Sedimentary Rocks. *Proc*. http://dx.doi.org/10.2118/124418-MS

Rojas, M.R., Muller, A.J., and Saez, A.E. 2008. Shear rheology and porous media flow of wormlike micelle solutions formed by mixtures of surfactants of opposite charge. Journal of Colloid and Interface Science 326 (1): 221-226. http://dx.doi.org/10.1016/js.jcis.2008.07.022

Rosen Milton J. Surfactants and Interfacial Phenomina. Third edition. Wiley. 2004.

Syaed, Mohammed A., Assem, Ahmed I. Nasr-El-Din. Hisham. Effect of Oil Saturation on the Flow of Emulsified Acids in Carbonate Rocks. *SPE Production & Operations*, 2014. http://dx.doi.org/10.2118/152844-PA

Skauge, Tormod, Kristine Spildo, Arne Skauge. 2010. Nano-sized Particles For EOR. *Proc*. http://dx.doi.org/10.2118/129933-MS

Sulman Esfir. M. Modern Catalytic Nanotechnologies for Sustainable Chemistry and Environmental Protection. International offshore and Polar Engineering Conference. 2010. ISOPE-I-10-238

Tombacz, E., M. Szekeres, I. Kertesz et al. 1996. pH-dependent aggregation state of highly dispersed oxide particles in aqueous medium. (in Hungarian). *Magyar Kemiai Folyoirat* 102 (1): 42-52. <Go to ISI>://WOS:A1996TW84400006.

Torsaeter, Ole, Shidong Li, Luky Hendraningrat. 2013. Enhancing Oil Recovery of Low-Permeability Berea Sandstone through Optimised Nanofluids Concentration. Presented at the SPE Enhanced Oil Recovery Conference, Kuala Lumpur, Malaysia, 2-4 July. SPE-165283-MS. http://dx.doi.org/10.2118/165283-MS.

Weston, J.S., Venkataramani., D., Aichele, C.P., Grady, B.P., Harwell, J., Resasco, D.,Pseudosolid, Shear-Thining Gel Formation in binary Dispersion of Metal Oxide Nanoparticles at Low Volume Fractions. *Langmuir*. 2014

Willianms, B.B., Gidley, J.L., and Schecherter, R.S., Acidizing Fundamentals, *SPE Monograph Series*, Vol.6, 1979

Wojtanowicz, A. K., Z. Krilov, J. P. Langlinais. 1987. Study on the Effect of Pore Blocking Mechanisms on Formation Damage. *Proc.* http://dx.doi.org/10.2118/16233-MS

Wojtanowicz, A. K., Z. Krilov, J. P. Langlinais. 1988. Experimental Determination of Formation Damage Pore Blocking Mechanisms (in *Journal of Energy Resources Technology* 110 (1): 34-42. http://dx.doi.org/10.1115/1.3231358

Yu, Jianjia, Cheng An, Di Mo et al. 2012. Study of Adsorption and Transportation Behavior of Nanoparticles in Three Different Porous Media. *Proc.* http://dx.doi.org/10.2118/153337-MS

Zakaria. A.S., Nasr-El-Din. H.A., A Novel polymer-Assisted Emulsified-Acid System Improves the Efficiency of Carbonate Matrix Acidizing. *SPE Journal*. 2015. http://dx.doi.org/10.2118/173711-PA